



# Using in-situ strain measurements to evaluate the accuracy of stress estimation procedures from fracture injection/shut-in tests

Yves Guglielmi<sup>a</sup>, Mark McClure<sup>b,\*</sup>, Jeffrey Burghardt<sup>c</sup>, Joseph P. Morris<sup>d</sup>, Thomas Doe<sup>e</sup>, Pengcheng Fu<sup>d</sup>, Hunter Knox<sup>c</sup>, Vince Vermeul<sup>c</sup>, Tim Kneafsey<sup>a</sup>, The EGS Collab Team

<sup>a</sup> Lawrence Berkeley National Laboratory, Berkeley, CA, USA

<sup>b</sup> ResFrac Corporation, Palo Alto, CA, USA

<sup>c</sup> Pacific Northwest National Laboratory, Richland, WA, USA

<sup>d</sup> Lawrence Livermore National Laboratory, Livermore, CA, USA

<sup>e</sup> TDoe Geo, Bellevue, WA, USA

## ARTICLE INFO

### Keywords:

DFIT  
Minifrac  
SIMFIP  
Collab

## ABSTRACT

Fracture injection/shut-in tests are commonly used to measure the state of stress in the subsurface. Injection creates a hydraulic fracture (or in some cases, opens a preexisting fracture), and then the pressure after shut-in is monitored to identify fracture closure. Different interpretation procedures have been proposed for estimating closure, and the procedures sometimes yield significantly different results. In this study, direct, in-situ strain measurements are used to observe fracture reopening and closure. The tests were performed as part of the EGS Collab project, a mesoscale project performed at 1.25 and 1.5 km depth at the Sanford Underground Research Facility. The tests were instrumented with the SIMFIP tool, a double-packer probe with a high-resolution three-dimensional borehole displacement sensor. The measurements provide a direct observation of the fracture closure signature, enabling a high-fidelity estimate of the fracture closure stress (ie, the normal stress on the fracture). In two of the four tests, injection created an opening mode fracture, and so the closure stress can be interpreted as the minimum principal stress. In the other two tests, injection probably opened preexisting natural fractures, and so the closure stress can be interpreted as the normal stress on the fractures. The strain measurements are compared against different proposed methods for estimating closure stress from pressure transients. The shut-in transients are analyzed with two techniques that are widely used in the field of petroleum engineering – the ‘tangent’ method and the ‘compliance’ method. In three of the four tests, the tangent method significantly underestimates the closure stress. The compliance method is reasonably accurate in all four tests. Closure stress is also interpreted using two other commonly-used methods – ‘first deviation from linearity’ and the method of (Hayashi and Haimson, 1991). In comparison with the SIMFIP data, these methods tend to overestimate the closure stress, evidently because they identify closure from early-time transient effects, such as near-wellbore tortuosity. In two of the tests, microseismic imaging provides an independent estimate of the size of the fracture created by injection. When combined with a simple mass balance calculation, the SIMFIP stress measurements yield predictions of fracture size that are reasonably consistent with the estimates from microseismic. The calculations imply an apparent fracture toughness 2–3x higher than typical laboratory-derived values.

## 1. Introduction

### 1.1. Overview

Fracture injection/shut-in tests are used to estimate the state of stress in the subsurface.<sup>1–11</sup> Injection propagates a hydraulic fracture, and the

pressure transient after shut-in is analyzed to estimate the fracture closure pressure, which is taken as an estimate for the minimum principal stress ( $S_{min}$ ). Alternatively, under certain conditions, injection may open a preexisting fracture, and in this case, the closure pressure may be interpreted as the normal stress on the fracture.<sup>8</sup> Fracture injection/shut-in tests are sometimes called minifracs, leakoff tests, or

\* Corresponding author.

E-mail addresses: [yguglielmi@lbl.gov](mailto:yguglielmi@lbl.gov) (Y. Guglielmi), [mark@resfrac.com](mailto:mark@resfrac.com) (M. McClure).

<https://doi.org/10.1016/j.ijrmms.2023.105521>

Received 31 January 2023; Received in revised form 3 May 2023; Accepted 2 July 2023

Available online 17 July 2023

1365-1609/© 2023 The Authors. Published by Elsevier Ltd. This is an open access article under the CC BY license (<http://creativecommons.org/licenses/by/4.0/>).

‘diagnostic fracture injection tests’ (DFITs).

Fracture injection test procedures vary significantly depending on context. In mining and civil engineering applications, fracture injection tests commonly utilize: (a) straddle packers to isolate small openhole sections, (b) coring and/or downhole imaging, (c) relatively small injection volumes, and (d) repeated injection cycles.<sup>8,11</sup> In oil, gas, and geothermal (OGG) applications, which usually involve deeper and larger boreholes, injection: (a) may utilize either openhole or cased/perforated sections, (b) rarely include coring, (c) usually do not use straddle packers, and (d) are often performed with a single injection cycle. In OGG applications, wells are rarely drilled with the primary purpose of performing stress estimation. Thus, wellbore orientation, construction, and test procedure are usually not ‘ideal’ from the perspective of estimating stress; interpretation must be robust to these challenges. In OGG applications with low permeability, fracture injection tests are often used to measure permeability and pore pressure, in addition to measuring the stress. Consequently, these tests use an extended shut-in lasting hours or days.<sup>10</sup>

Pressure measurements during fracture closure are used to estimate the closure stress. However, different procedures are available in the literature, and these procedures may yield significantly different results. This has led to ongoing controversy in the literature.<sup>12–23</sup> The discrepancy from different interpretation procedures creates a need for independent assessment of their accuracy.

This paper analyzes results from fracture injection tests performed at the EGS Collab project at Sanford Underground Research Facility (SURF) in South Dakota, USA.<sup>24,25</sup> The fracture injection tests were instrumented with the SIMFIP tool (Step-Rate Injection Method for Fracture In-Situ Properties), which measures 6-component displacements during and after fluid injection.<sup>26–28</sup> The SIMFIP displacement measurements provide a mechanical measurement of fracture closure during shut-in, which can be used to derive an independent estimate of fracture closure stress.

This paper primarily focuses on comparing two procedures – the ‘tangent’ and ‘compliance’ procedures.<sup>12,16</sup> These methods are chosen because: (a) they are widely used in OGG applications, (b) there is ongoing literature disagreement regarding their accuracy, and (c) they often yield significantly different stress estimates.

In mining and civil engineering applications, the tangent and the compliance methods are not commonly used.<sup>8</sup> and <sup>11</sup> review the most widely used methods. Testing all of these methods would be beyond the scope of the present paper. However, for completeness, in Section 3.3, we include comparison with two procedures – (a) the method of <sup>1</sup>; and (b) the ‘first deviation from linearity’ on a square root of time or G-function plot.<sup>7,9,29</sup>

## 1.2. Fracture toughness and net pressure

In a propagating hydraulic fracture, the ‘fracture propagation pressure’ is the pressure measured in the wellbore during injection as the fracture propagates.<sup>9</sup> The propagation pressure is higher than the minimum principal stress because: (a) the pressure in the fracture must exceed the stress magnitude to open the fracture and overcome the formation’s fracture toughness, and (b) pressure can be elevated by wellbore friction, near-wellbore pressure drop, and/or pressure gradient along the fracture. To estimate the stress, the pressure is monitored after shut-in to identify the ‘fracture closure pressure,’ which, for a newly forming fracture, is interpreted as being equal to  $S_{min}$ .<sup>7,9,29</sup> The ‘initial shut-in pressure’ (ISIP) is interpreted as an estimate of pressure in the fracture during propagation.<sup>9</sup> In horizontal wells, near-wellbore tortuosity can elevate pressure for tens of minutes after shut-in, and so alternatively, the ‘effective ISIP’ may be used.<sup>16</sup>

The ‘net pressure’ is defined as the difference between the fluid pressure in the fracture and the normal stress on the fracture. Larger net pressure implies greater effective fracture toughness, greater aperture, and lower surface area.<sup>30</sup> Laboratory-derived values of fracture

toughness imply that net pressure should be very low (<0.5–1 MPa) for cracks larger than a few feet.<sup>9</sup> However, in-situ measurements suggest that toughness may exhibit scale-dependence,<sup>31–33</sup> and that in-situ net pressure are usually on the order of 2–3 MPa or more (<sup>34</sup>; Section 6-7.2 from <sup>30,35</sup>).

A variety of different processes have been proposed to explain elevated field-scale values of fracture toughness (Section 5-4.5 from <sup>36</sup>; Section 6-7.2 from <sup>30</sup>; Section 2.8 from <sup>33,37</sup>). Independently, geologists have hypothesized that fracture toughness may be scale-dependent, based on rock outcrop observations.<sup>31,32</sup> Numerical modeling matches to high-quality diagnostics from field-scale hydraulic fracturing datasets in shale usually yield apparent toughness estimates that are 2–3x or more above typical laboratory values.<sup>38–40</sup>

The SIMFIP measurements of fracture closure from the EGS Collab project provide a high-fidelity measurement of fracture closure. In Section 3.4, values of apparent toughness are calculated from the observations. The values are combined with mass balance calculations to compare with microseismic observations of fracture size.

## 1.3. G-function plotting techniques

Many procedures for identifying fracture closure are based on plotting pressure versus a function of time that has been derived to represent the scaling of leakoff rate with time. If the fracture is assumed to have formed instantaneously, the leakoff rate from the fracture is expected to scale with the inverse of the square root of time.<sup>41</sup> Therefore, if the fracture stiffness is constant prior to closure, a plot of pressure versus square root of time should generate a straight line (Appendix A from <sup>15</sup>). As explained by <sup>7</sup>, closure causes a ‘deviation from linearity’ that can be used to identify fracture closure and estimating stress: “the pressure decline approaches a linear relation with the square root of time since shut-in began ... when the fracture closes a distinct change in slope may be seen ... the break can be either way and depends on the relative relationship of the variables of the fracture and the reservoir.”

G-function plotting techniques have been used for stress estimation in the oil and gas industry since the 1980s. The G-function is an improvement over the ‘square root of time’ plotting technique because the derivation accounts for non-instantaneous propagation of the fracture over time – which causes the ‘duration of leakoff’ to be different at different locations along the fracture.

The G-function is a dimensionless function of time derived such that – given certain simplifying assumptions (such as Carter leakoff) – it is linearly proportional to the volume of fluid leaked off from the fracture prior to the contacting of the fracture walls.<sup>42,43</sup> This property allows G-function plotting techniques to be used to estimate not only stress, but also fracture geometry and the leakoff coefficient<sup>44,45</sup>; Section A.3 from <sup>16</sup>.

The G-function is defined as:

$$G(\Delta t) = \frac{4}{\pi} (g(\Delta t) - g(\Delta t = 0)). \quad (1)$$

In low permeability rock, the g-function is defined as:

$$g(\Delta t) = \frac{4}{3} \left[ \left( 1 + \frac{\Delta t}{t_e} \right)^{1.5} - \left( \frac{\Delta t}{t_e} \right)^{1.5} \right]. \quad (2)$$

$\Delta t$  is duration of shut-in, and  $t_e$  is the duration of injection.<sup>46</sup> provides a succinct derivation of Equation (2), based on the original derivation from <sup>42</sup>.

## 1.4. Compliance and tangent methods for identifying fracture closure

To demonstrate the compliance and tangent methods, Figs. 1 and 2 show interpretations of a Utica/Point Pleasant shale DFIT (the figures are reproduced from <sup>16</sup>). The test was performed from the toe of a

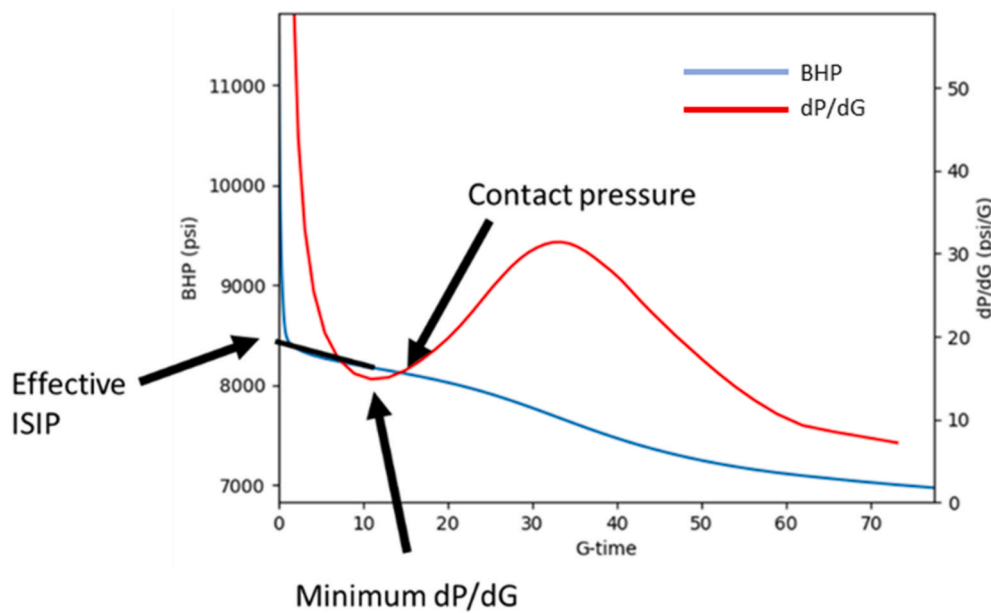


**Fig. 1.** Example of a compliance method stress estimate. The blue curve shows pressure, and the red curve shows  $dP/dG$ . Data taken from a fracture injection test in the Utica/Point Pleasant Shale.<sup>16</sup> (For interpretation of the references to colour in this figure legend, the reader is referred to the Web version of this article.)

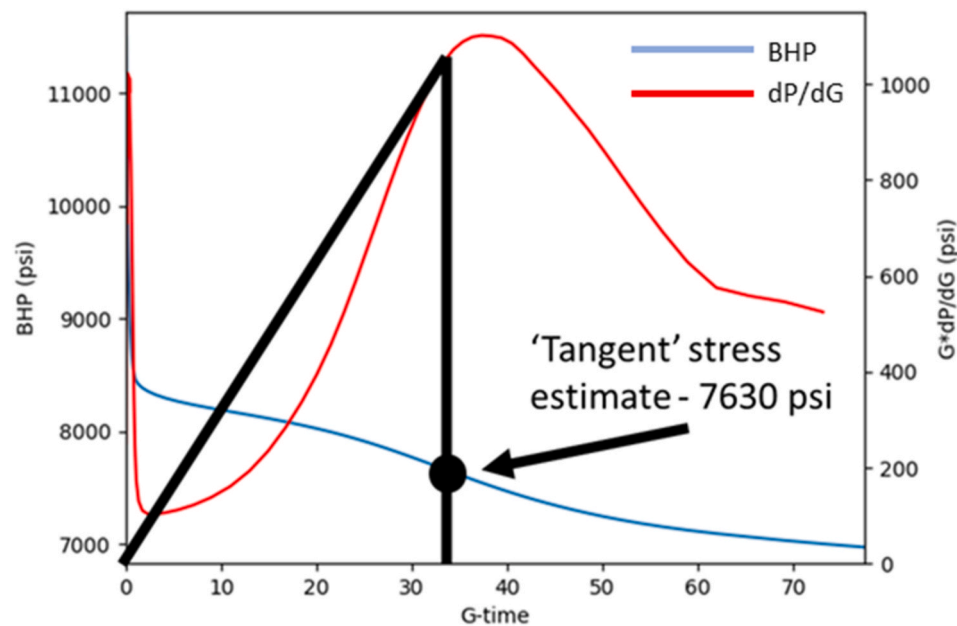


**Fig. 2.** Example of a tangent method stress estimate. The blue curve shows pressure, and the red curve shows  $G \cdot dP/dG$ . Data taken from a fracture injection test in the Utica/Point Pleasant Shale.<sup>16</sup> (For interpretation of the references to colour in this figure legend, the reader is referred to the Web version of this article.)

horizontal well, with a total volume of  $7.37 \text{ m}^3$  (46.4 bbl) of fluid with an injection rate of  $0.013 \text{ m}^3/\text{s}$  (5 bbl/min). The pressure drops by roughly 20.7 MPa (3000 psi) in the first hour of shut-in. This pressure drop corresponds to the dissipation of near-wellbore tortuosity and does not indicate closure or yield a stress estimate.

Following the procedure from<sup>16</sup>, the straight section of the pressure versus G-time plot can be extrapolated back to the y-intercept to estimate the pressure in the far-field fracture at shut-in (the so-called effective instantaneous shut-in pressure, or effective ISIP). In Fig. 1, the effective ISIP is 57.4 MPa (8330 psi). The magnitude of the near-wellbore tortuosity is approximately equal to the difference between the 'literal' ISIP (equal to roughly 11,300 psi in Fig. 1) and the effective ISIP.

<sup>35</sup> reviewed 62 DFITs performed in various shale formations across North America and found that – in horizontal wells drilled in the direction of  $S_{\text{hmin}}$  – the early-time pressure drop varied between 5 and 40 MPa. In contrast, in vertical wells, the early-time pressure-drop was usually less than 1 MPa. The difference arises because in vertical wells, fractures can form longitudinally along the wellbore, resulting in little or zero near-wellbore tortuosity (unless in a reverse faulting regime), but in horizontal wells drilled in the direction of  $S_{\text{hmin}}$ , the far-field fracture orientation is transverse to the well orientation.

In Fig. 1, at around G-time of 17 and 55.8 MPa (8100 psi), the pressure curve deviates from a straight line and begins to decrease more rapidly. This corresponds to an upward deflection on the plot of  $dP/dG$ . The 'compliance method' identifies the point where  $dP/dG$  has

increased appreciably above its minimum value and labels this point the ‘contact pressure.’ The compliance stress estimate is defined as being equal to the contact pressure minus 0.5 MPa (75 psi). The subtraction of 0.5 MPa accounts for the effect of fracture roughness, which causes the walls to contact at a pressure slightly higher than the normal stress. Therefore, in this case, the compliance method estimate is 55.3 MPa.

<sup>16</sup> recommend picking the contact pressure when  $dP/dG$  has increased 10% above its minimum value. The ‘10% increase’ and ‘subtract 0.5 MPa’ guidelines are both rules of thumb, developed to be simple and practical. The procedure yields good accuracy when compared with detailed numerical simulation matches to real data.<sup>15,16</sup> As with other graphical stress estimation techniques, there is sometimes a modest degree of subjectivity in making the ‘compliance’ pick on real data. The stress estimate has at least  $\pm 1$  MPa of uncertainty, which is unavoidable, given the complexity of real-life fracturing process and the inherent heterogeneity of in-situ stress.<sup>35</sup> note that in some cases,  $dP/dG$  inflects upwards and then inflects downwards, but never quite reaches a maximum; in these cases, closure may still be picked with ‘adequate’ confidence (an example is shown in Fig. 17a, below).

The increase in  $dP/dG$  visually corresponds to a deviation from linearity, and so the compliance procedure is somewhat analogous to the classical stress estimation technique of estimating stress at the first deviation from linearity described by <sup>29</sup> and <sup>7</sup>. However, the compliance method differentiates between the early-time ‘near-wellbore tortuosity’ and the subsequent occurrence of fracture closure. The ‘first deviation from linearity’ method could mistakenly pick closure during the dissipation of the near-wellbore tortuosity. If applied to the test in Fig. 1, this would result in a significant overestimate of the stress. As discussed in Section 3.3, the method of <sup>1</sup> would also be affected by this issue and would significantly overestimate stress if applied to the test in Fig. 1.

The tangent method stress estimate relies on a plot of  $G \cdot dP/dG$  (Fig. 2). A straight line is drawn from the origin to the tangent of the  $G \cdot dP/dG$  curve. The stress estimate is equal to the point where the  $G \cdot dP/dG$  curve deviates downward from the straight line.

In this example, the tangent method estimate is 52.6 MPa (7630 psi), 2.7 MPa (395 psi) less than the compliance method estimate. The implied net pressure (the pressure in the fracture minus the normal stress) is  $(57.4 - 55.3) = 2.1$  MPa with the compliance method and  $(57.4 - 52.6) = 4.8$  MPa with the tangent method.

The tangent method yields systematically lower stress estimates than the compliance method. A review of 62 DFITs from <sup>35</sup> found that the tangent method was about 3 MPa lower, on average, implying a 2.5x higher net pressure. In some cases, the methods differed by 5 MPa or more.

<sup>15</sup> provide a mathematical framework for explaining how and why the pressure trend changes with closure. If the permeability is very low (less than approximately 10 microdarcies), then the fracture will remain effectively infinite conductivity after closure. In this case, the system can be described with a simple lumped parameter model. Under these conditions, it can be derived that<sup>15,16</sup>:

$$\frac{dP}{dG} = \frac{1}{C_t} \frac{dV}{dG}, \quad (3)$$

where  $P$  is pressure,  $G$  is G-time,  $C_t$  is the storage coefficient of the wellbore/fracture system, and  $V$  is the volume of fluid in the wellbore/fracture system. The storage coefficient is defined as the volume of fluid released from the system per increment of pressure decrease. The system storage coefficient includes the wellbore storage coefficient (primarily controlled by the compressibility of the fluid in the well) and the fracture storage coefficient (primarily controlled by changes in fracture volume with pressure).

As long as the walls are out of contact, then according to linear elasticity, the fracture storage coefficient should be approximately constant (<sup>47</sup>; Equation 9-21 from <sup>43</sup>; Section 8.13 from <sup>48</sup>). The G-function was derived by <sup>42</sup> specifically to have the property that  $\frac{dV}{dG}$  will be

constant, as long as leakoff is consistent with the Carter leakoff model (ie, leakoff rate at a location is approximately equal to the inverse of the square root of time). The Carter leakoff model is only valid if pressure in the fracture is approximately constant. As pressure decreases during shut-in, the Carter leakoff assumption becomes increasingly inaccurate, and  $\frac{dV}{dG}$  begins to gradually decrease as leakoff occurs more slowly than would be expected from Carter leakoff.

At early time, before significant pressure decrease, and while the fracture walls are still out of contact, both terms in Equation (3) are constant and so  $\frac{dP}{dG}$  is constant, resulting in a straight line on the  $P$  versus  $G$  plot (or equivalently, the  $P$  versus  $\sqrt{t}$  plot).

When the fracture walls contact, the fracture becomes stiffer, which decreases the system storage coefficient, resulting in an increase in  $\frac{dP}{dG}$ . This is why <sup>15,16</sup> recommend picking the ‘contact pressure’ at the point when the derivative has increased from its minimum. The fracture walls do not contact instantaneously everywhere, and they have some residual aperture at contact caused by roughness. Thus, the ‘compliance method’ interpretation is to estimate stress at 0.5 MPa (75 psi) less than the contact pressure.

The  $\frac{dP}{dG}$  curve eventually peaks and goes back down. The peak occurs because as the pressure decreases, Carter leakoff becomes an increasingly invalid assumption, and so rather than remaining constant,  $\frac{dV}{dG}$  decreases progressively to zero.

As discussed by <sup>16,35</sup>, a significant percentage of tests exhibit monotonically decreasing  $dP/dG$ , rather than the ‘S’ shape seen in Fig. 1. This may occur for two primary reasons: (a) the fracture closes rapidly after shut-in, and/or (b) near-wellbore tortuosity is so strong or takes so long to dissipate that it covers the actual transient. In a horizontal well where near-wellbore tortuosity may be strong,<sup>16,35</sup> recommend against making a stress estimate, since there is not an unambiguous indication of closure. In a vertical well or in a situation where we otherwise expect to see minor near-wellbore tortuosity, then we may interpret the test as representing ‘rapid closure’ and use the ‘first deviation from linearity’ approach. In this scenario, the uncertainty in the stress estimate is considered relatively high, because of the risk that near-wellbore tortuosity or other brief transient effects occur simultaneously with fracture closure.

<sup>16</sup> developed an alternative to the G-function that scales with cumulative leakoff volume, but accounts for changing pressure in the fracture over time (ie, does not assume Carter leakoff). Using this concept, it is possible to construct a ‘relative stiffness’ plot. On this plot, the contact pressure can be estimated from when stiffness is observed to increase appreciably. Fig. 3 shows the relative stiffness plot constructed

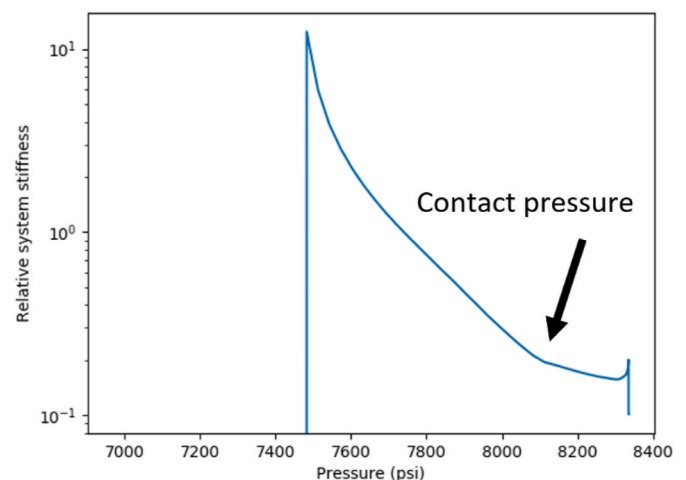


Fig. 3. Example of a relative stiffness versus pressure plot. Data taken from the same Utica/Point Pleasant Shale fracture injection test that is shown in the previous figures. Relative stiffness is a unitless quantity.



from the same data as Figs. 1 and 2. The stiffness increases at 55.8 MPa (8100 psi), consistent with the compliance method pick seen in Fig. 1.

### 1.5. Other examples in the literature

Several recent papers have performed explicit comparisons between methods for estimating closure stress.

<sup>20</sup> described a series of minifracs performed with in-situ strain measurements at the Grimsel project. They found that the compliance-based estimates were reasonably accurate, and that the tangent-method estimates were significantly too low. These tests typically exhibited a ‘monotonic dP/dG’ signature, a special case discussed in Section 1.4. They tested a method similar to the procedure from <sup>1</sup> and found that it yielded accurate interpretations.

<sup>22</sup> analyzed a set of minifrac tests with five different stress estimation procedures. They did not use strain measurements to independently assess accuracy; they solely performed a comparison between different procedures. The tangent method was an outlier, yielding much lower results than the other methods. In some cases, the tangent method estimates were so low that they violated constraints based on the frictional strength of the rock. The compliance method estimates were the second-lowest of the five techniques, but much closer to the others than the tangent method.

<sup>15</sup> compared shut-in transients with tiltmeter measurements from the DOE M-Site project. They found that the tangent method yielded an underestimate, and that the compliance method accurately picked closure.

In contrast, <sup>17</sup> also analyzed the tiltmeter measurements from the M-Site project and argued that the results supported the use of the tangent method. The apparent difference from the interpretation of <sup>15</sup> was related to how they estimated stress from the deformation measurements. They did not use the ‘x-intercept’ approach explained in Section 2.3 (Figure 9A-4 from <sup>43</sup>). Further discussion is provided by <sup>19</sup>

In tests from vertical wells with little or no near-wellbore tortuosity, fracture reopening pressures can provide a useful independent estimate of  $S_{min}$ . For example, <sup>49</sup> analyzed microfrac tests performed from vertical wells in shale. In their tests, the tangent method interpretations were consistently several MPa lower than the fracture reopening pressures.

<sup>21</sup> compared the tangent and compliance methods and argued that the tangent method yielded the correct stress estimate. The discussion from <sup>21</sup> was based on heuristic arguments related to stress profiles derived from well logs and measurements of fracture height growth.

<sup>23</sup> applied the tangent and compliance methods to interpret microfrac tests performed at the laboratory scale. The tangent method interpretations were around 3 MPa lower than the  $S_{min}$  imposed on the rock samples. The compliance method interpretations were about 1 MPa lower than the imposed  $S_{min}$ .

## 2. Methods

### 2.1. Project background

In this study, we analyze fracture injection tests performed as part of the EGS Collab project at Sanford Underground Research Facility (SURF) in South Dakota, USA. <sup>24,25,27,60</sup>

Numerous fracture injection tests were performed at the Collab project. However, most involved brief shut-in, followed by flowback. For this study, we used only tests that had extended shut-in periods and simultaneous SIMFIP measurements. There were four fracture injection tests that met these requirements, and these are the tests included in this study. The E1-I 164 Test 2 probably had slight leakage into a grouted, nearby observation well, as discussed below, but was nevertheless included in the study.

Of the four tests, two were performed in a borehole drilled from the 4100' level of the mine (~1.25 km deep), and two were performed in a borehole drilled from the 4850' level of the mine (~1.5 km deep –

Table 1). These depths are referenced to a particular reference location in the mine shaft and are not referenced precisely to the geodetic datum depth. The borehole on the 4850' level, E1-I, was 69 m long and slightly dipping from horizontal while the 4100' borehole, TV 4100', was approximately 50 m long and vertical. The E1-I tests at the 4850' level were performed at a measured depth of 164 ft (50 m) from the wellhead. The E1-I well was drilled in approximately the direction of  $S_{hmin}$ . The tests at the 4100' level were performed at a measured depth of 32 ft (9.8 m) and 148 ft (45.1 m) (TV Test 4 and TV Test 7).

The stress state in the vicinity of the E1-I tests was previously estimated from tests performed in nearby borehole as part of the Kismet project. <sup>25,50,51</sup> The vertical stress magnitude was estimated to be around 41.8 MPa. The magnitudes of  $S_{Hmax}$  and  $S_{hmin}$  have been estimated to be around 34.0 and 21.7 MPa. As noted in Section 3.1, the SIMFIP measurements suggest that  $S_{hmin}$  is 21.4 MPa, which is close to the Kismet estimate. Over time, fluid has drained into the mineshaft, causing a localized region of depleted pore pressure. The in-situ magnitude of stress may also be significantly depleted by this depletion. There is likely a spatial gradient in both pore pressure and stress towards the mineshaft.

In the E1-I 164 tests, there were three injection/shut-in periods. The third injection period caused the fracture to intersect an offset production well at a distance of 10 m.

In the well at the 4100' interval, a total of eight injections were performed, all with the SIMFIP probe. Of these, most involved brief shut-in followed by flowback. The tests suggested significant stress variation along the borehole, evidently caused by differences in lithology. Of the tests in the 4100' interval, Tests 4 and 7 used extended shut-ins, and these are the two analyzed in this study.

### 2.2. SIMFIP tool

The SIMFIP tool contains a 6-component displacement sensor for measuring deformation during and after fluid injection. The injection interval is isolated by packers on each side, separated by 2.41 m, and the displacement sensor is placed in the center. The displacement sensor is an aluminum cage (0.24 m and 0.1 m diameter) connected to two 0.58 m elements that enable clamping to the borehole wall (Points A and B in Fig. 4). The sensor measures the relative borehole wall displacement between the anchors, which are 1.4 m apart. When clamped, the cage is disconnected from the packer system, which enables it to measure deformation independently from the packer system. The resolution of the measurements is at the micrometer scale, and the range is a few millimeters. The system enables continuous and simultaneous measurement of the three-dimensional borehole wall displacements, injection rate, and injection pressure.

Examples of the SIMFIP test procedure are provided by <sup>26,52</sup> and <sup>53</sup>. SIMFIP tests typically begin with a calibration injection. Pressure is increased in steps to a pressure safely below the fracture initiation pressure, and then the pressure is stepped back down. The deformation response is used to calibrate the tool's response in the absence of fracturing. Usually, the displacements are reversible when the pressure is stepped back down.

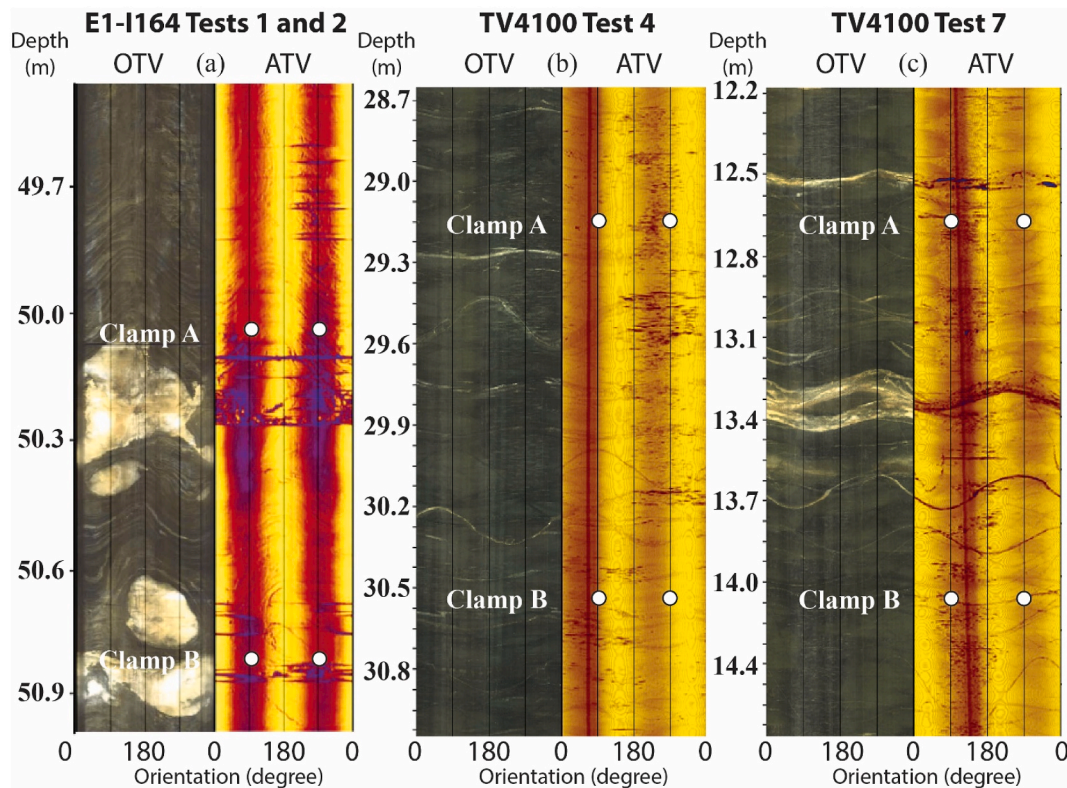
After the calibration injection, one or more injection steps are performed at higher rate and pressure, to create and propagate a hydraulic fracture. At the beginning of fracturing, the displacement distribution is often complex because of localized deformation associated with fracture initiation. However, with further injection (and during subsequent injection cycles), the displacement measurements become dominated by the primary deformation mode in the near-wellbore region (within a few meters).

The SIMFIP can produce reliable data when fractures make an angle  $> \sim 10^\circ$  with the borehole. This is the case in the four tests presented in this paper. Indeed, the fracture is almost perpendicular to the borehole in the E1-I 164 tests, while reactivated fractures make angles of 12 and  $36^\circ$  with borehole respectively in the two tests from the 4100' interval (see Fig. 5).

**Table 1**

Summary of the geological setting of each test.

Test	Depth of the wellhead (m)	Borehole Orientation		Fractures (from Optical and Acoustic logs)			Geology
		Azimuth	Inclination	Number	Dip direction	Dip angle	
E1-I 164 Test 1	1490.5	02°	9.3°	0			Intact foliated metamorphic rock
E1-I 164 Test 2	1490.5	02°	9.3°	1	Hydro-fracture Dip direction (dd) 159° Dip angle (da) 83°		Intact foliated metamorphic rock with one hydraulic fracture (HF) initiated during the test
TV4100' Test 4	1278	0°	90°	~13	~3 fractures directions dd 180–240° da 45–55° dd 110–120° da 10–20° dd 0–10° da 60°		Foliated metamorphic rock with ~13 initially closed and/or cemented natural fractures
TV4100' Test 7	1262	0°	90°	~20	~3 fractures directions dd 100–130° da 20–40° dd 70° da 49° dd 199° da 43°		Foliated metamorphic rock with ~20 initially closed and/or cemented natural fractures

**Fig. 4.** Pre-tests logs (OTV – Optical Tele Viewer, ATV – Acoustic Tele Viewer (modified from <sup>27</sup>).

### 2.3. Estimating the fracture closure stress from SIMFIP measurements

To estimate the fracture closure stress (ie, the normal stress on the fracture), the fracture-normal displacement should be plotted versus pressure (Fig. 6).

When a crack is mechanically open and not propagating, there is an approximately linear relationship between deformation and pressure, as given by the equation (<sup>47</sup>; Equation 9-21 from <sup>43</sup>; Section 8.13 from <sup>48</sup>):

$$\bar{W} = \frac{P - Sh_{min}}{S_f} = (P - \sigma_n)C_f, \quad (4)$$

where  $\bar{W}$  is the average fracture width (defined as the crack volume divided by area),  $S_f$  is the fracture stiffness,  $C_f$  is the fracture compliance (equal to the reciprocal of fracture stiffness), and  $\sigma_n$  is the normal stress on the fracture.

The fracture walls contain asperities that contact during closure, creating a backstress that nonlinearly increases stiffness.<sup>54</sup> The asperities contact at a width  $\bar{W}_c$  that is some fraction of the maximum width reached during injection. If the crack was perfectly smooth, then  $\bar{W}_c$  would be equal to zero, and the straight line would extend all the way to zero on the x-axis of Fig. 6. With nonzero  $\bar{W}_c$ , the curve deviates from the straight line and curves to asymptotically approach zero (or possibly, a small residual width) as pressure decreases below the normal stress. Comparison between Fig. 6 and Equation (4) shows that the x-intercept of the straight line is equal to normal stress. It might be tempting to identify ‘closure/reopening’ as the point where the displacement visually deviates from zero. However, the progressive, asymptotic reduction in aperture with falloff continues at pressures much lower than the fracture normal stress.

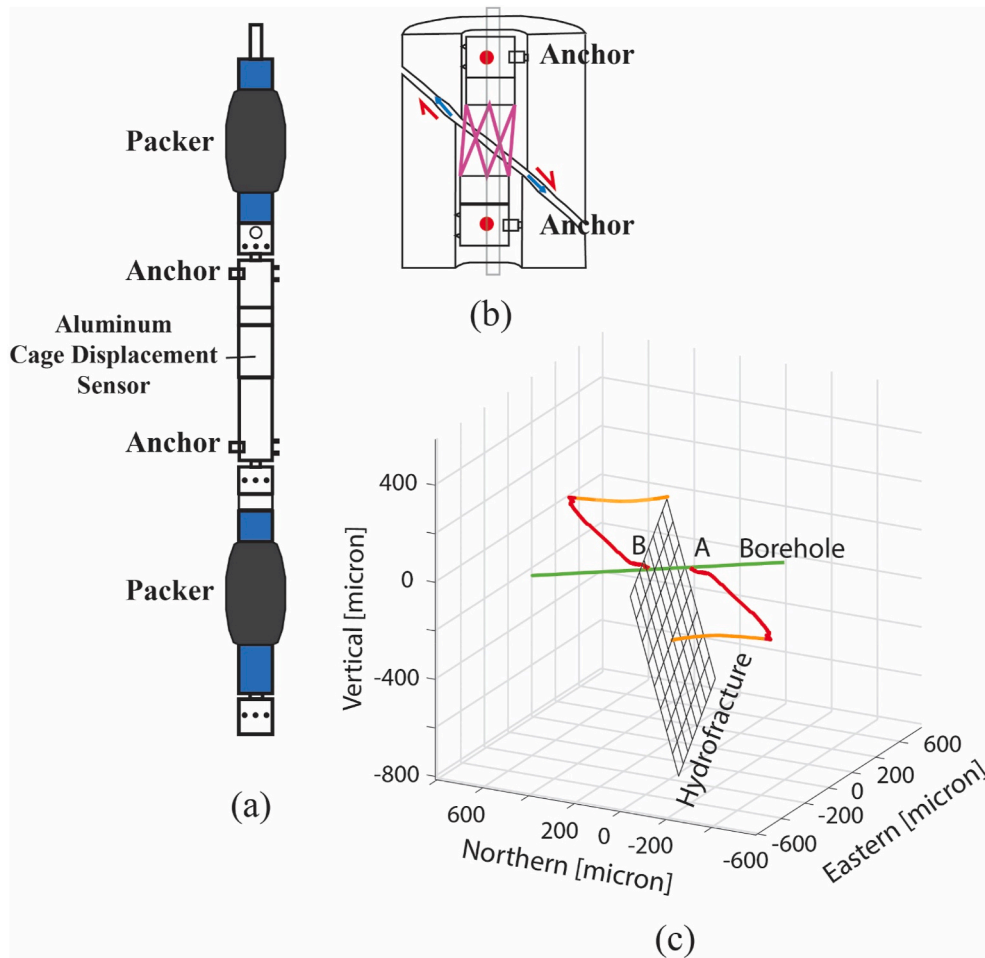


**Fig. 5.** SIMFIP probe. (a) Design of the probe; (b) Schematic concept of the borehole three-dimensional relative displacement between anchors A and B; (c) Example of a SIMFIP displacement signal captured across the activated hydrofracture during E1-I 164 Test 2. Red segment is the displacement during injection and growth of the fracture. Orange segment is the displacement during shut-in (modified from <sup>27</sup>). (For interpretation of the references to colour in this figure legend, the reader is referred to the Web version of this article.)

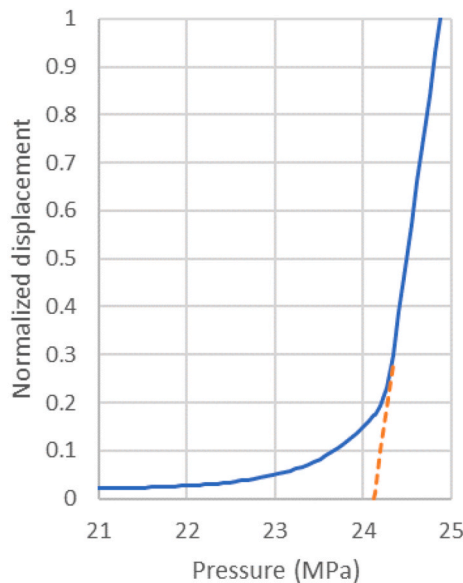


**Fig. 6.** Schematic of hydraulic fracture reopening/closure. Based on Figure 9A-4 from <sup>43</sup>. The orange dashed line shows the extrapolation of the 'open fracture' curve back to the fracture normal stress (ie, the fracture closure stress), as per Equation (4). (For interpretation of the references to colour in this figure legend, the reader is referred to the Web version of this article.)

### 3. Results and discussion

#### 3.1. E1-I 164 interval

E1-I 164 Test 1 involved 10 min of injection at 0.2 l/min, followed by an extended shut-in (Fig. 7). A power outage ended the SIMFIP recording once the pressure had reached 22.2 MPa. The pressure measurements continued until reaching a minimum of 20 MPa. E1-I 164 Test 2 involved 57 min of injection at up to 0.4 l/min<sup>27</sup>, followed by a 15 h shut-in (Fig. 8). E1-I 164 Test 3 involved injection at 3 l/min until the fracture intersected an offset production well, as observed by a down-hole camera in the production well.

The interval in the E1-I tests was notched prior to the tests, in order to promote breakdown. However, the SIMFIP measurements suggest initiation probably did not occur from the notch. During initiation at the start of Step 1, the SIMFIP observed microshearing on a preexisting foliation plane until reaching 112% of the estimated  $Sh_{min}$ , followed by initiation and opening-mode displacement. Overall, the E1-I tests are believed to have predominantly created an opening mode hydraulic fracture. Therefore, the closure stress can be interpreted as representing the magnitude of the minimum principal stress.

A detailed microseismic array provided information on the far-field fracture geometry, which was approximately planar and perpendicular to  $Sh_{min}$ , with some interaction with natural fractures, and possibly a few different discrete propagation planes.<sup>27,55,56</sup>

Because of the early loss of recording, the SIMFIP measurements from Test 1 are insufficient to enable an estimation of the normal stress. The SIMFIP measurements from the Test 2 reopening and closure and the Test 3 reopening provide the best data for estimating stress. In these



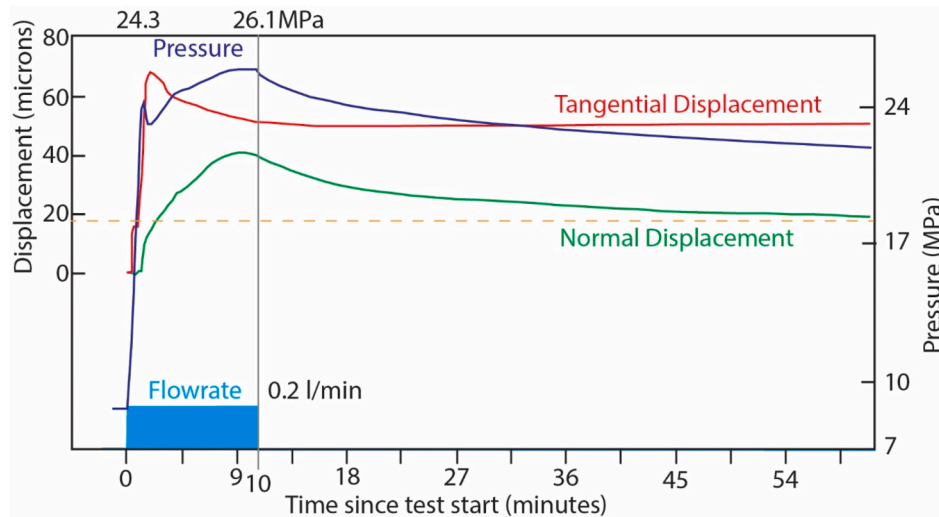


**Fig. 7.** SIMFIP displacement normal and tangential to the activated fracture during E1-I 164 Test 1. Displacements are plotted with injection chamber pressure and injection flowrate (note that only a part of the shut-in is plotted on this graph). The tangential displacement is the absolute shear displacement regardless of its direction in the fracture plane.

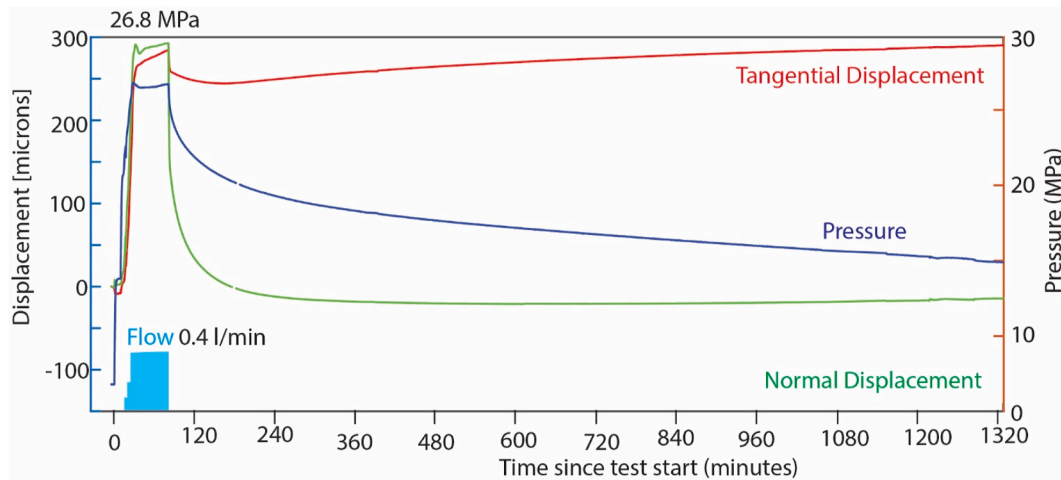


**Fig. 8.** SIMFIP displacement normal and tangential to the activated fracture during E1-I 164 Test 2. Displacements are plotted with injection chamber pressure and injection flowrate. The tangential displacement is the absolute shear displacement regardless of its direction in the fracture plane.

tests, the measured reopening and shut-in lie on top of each other. The curves all have an x-intercept stress estimate around 21.4 MPa (Fig. 9). As the pressure drops further, the fracture continues to gradually close and stiffen, as the fracture closes down on asperities.

The final asymptote in displacement is not required to occur at a measured value of zero. Irreversible displacement can occur during injection, resulting in an apparent offset from zero. As a result, the 'x-intercept' stress estimate should be based on drawing a tangent to the

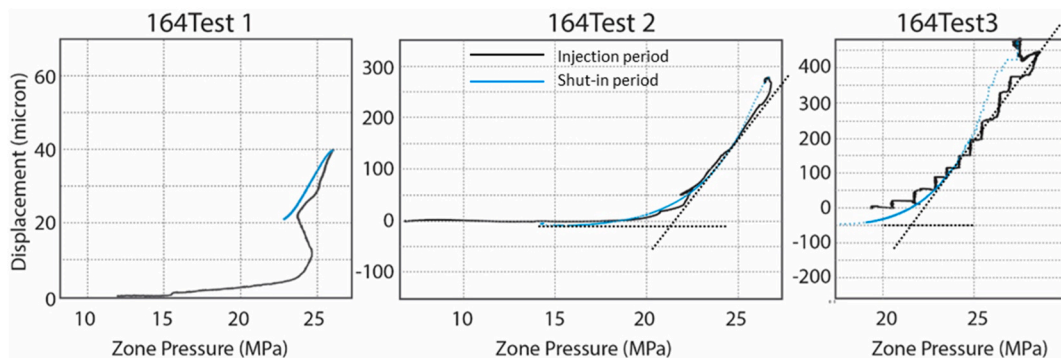


**Fig. 9.** SIMFIP displacement normal to the activated fracture versus zone pressure for the E1-I 164 tests. Black is the injection period, blue is the shut-in period. The black dashed lines have been added to show how stress can be estimated from the plot, as shown in Fig. 6. The intercept occurs at around 21.4 MPa in both Tests 2 and 3. (For interpretation of the references to colour in this figure legend, the reader is referred to the Web version of this article.)



long-term asymptote on the plot, rather than at the literal value of ‘zero’ on the plot.

The displacement data from the Test 1 shut-in cannot be interpreted to estimate stress using the technique shown in Fig. 6, because the test ended before we could identify the location of the final asymptote in displacement. The bending of the curve suggests that it may have occurred at a y-axis value around 19  $\mu\text{m}$ , implying an ‘x-intercept’ at a pressure similar to Tests 2 and 3. However, without the measurements, this is not known with certainty.

Fig. 10 shows the G-function and relative stiffness plots from the E1-I 164 Test 1 shut-in. The  $dP/dG$  plot indicates a contact pressure of 21.9 MPa, for a ‘compliance method’ stress estimate of 21.4 MPa – the same as the ‘x-intercept’ stress estimate from the SIMFIP measurements. The relative stiffness plot shows an upward deflection at a slightly higher pressure as the  $dP/dG$  plot, 22.1 MPa. Conversely, the ‘tangent method’ interpretation of the  $G^*dP/dG$  plot is that the fracture never closed during the duration of the shut-in.

If the shut-in had been performed for longer duration in E1-I 164 Test 1, it is certain that a tangent point would have eventually been reached and that the ‘tangent method’ stress estimate would have been lower than the final measured pressure. It is a mathematical requirement that the  $G^*dP/dG$  curve must always eventually yield a ‘tangent’ point, given a sufficiently long shut-in period. As time goes to infinity, the pressure derivative goes to zero, which causes the  $G^*dP/dG$  curve to approach zero. At G-time equal to zero,  $G^*dP/dG$  must be equal to zero. Thus, the  $G^*dP/dG$  curve must always increase from zero, and then eventually bend back down to zero. This implies that there is always a point when a straight line from the origin is tangent to the curve, creating a ‘tangent closure pick.’ For detailed analysis of the late-time asymptotic behavior of shut-in pressure transients from fracture injection tests, refer to

Ref. 46.

The  $dP/dG$  curve in E1-I 164 Test 2 is monotonically decreasing (Fig. 11). According to the compliance procedure from <sup>16</sup>, a monotonically decreasing  $dP/dG$  curve indicates either: (a) rapid closure, or (b) excessive near-wellbore tortuosity. Because there is not an indication of strong near-wellbore tortuosity in this dataset, the best interpretation is the ‘rapid closure’ interpretation. The ‘rapid closure’ stress estimate is equivalent to the effective ISIP; it does not yield a precise stress estimate, and so ‘compliance stress estimate’ is an inexact range from roughly 20.7–24.1 MPa.

The  $G^*dP/dG$  plot never reaches a tangent point or maximum, and so the ‘tangent method’ interpretation is that the fracture never closed, reaching a minimum pressure of 15.2 MPa. The SIMFIP estimate of 21.4 MPa is within the range of the compliance method ‘rapid closure’ interpretation. The tangent method interpretation (that the stress is less than 15.2 MPa) is far too low.

‘Rapid closure’ in Test 2 was evidently caused by either: (a) intersection with a relatively conductive natural fracture, or (b) possible leakoff into an offset observation well. The offset observation well was grouted, and so supposedly sealed to flow. However, distributed temperature sensing (DTS) measurements in the observation well indicated a small temperature change, suggesting that some fluid may have leaked off into the well.

### 3.2. TV 4100’ interval

In TV 4100’ Test 4 Cycle 1, injection was performed at 1.2 l/min for 10.48 min, followed by a 7-h shut-in (Fig. 12). The SIMFIP measurements suggest reactivation (opening and shearing) on a fracture with 236°/54° dip direction/dip angle. At the fracturing pressure during

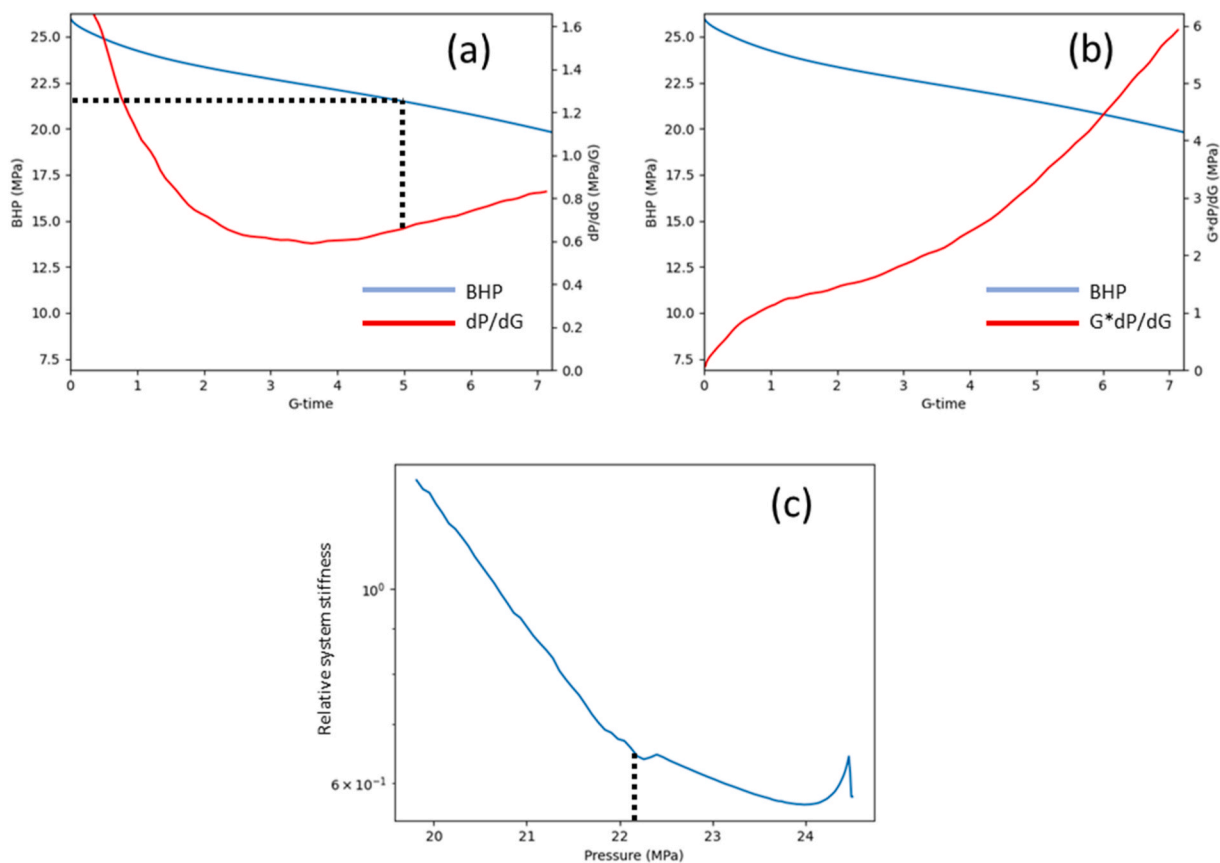
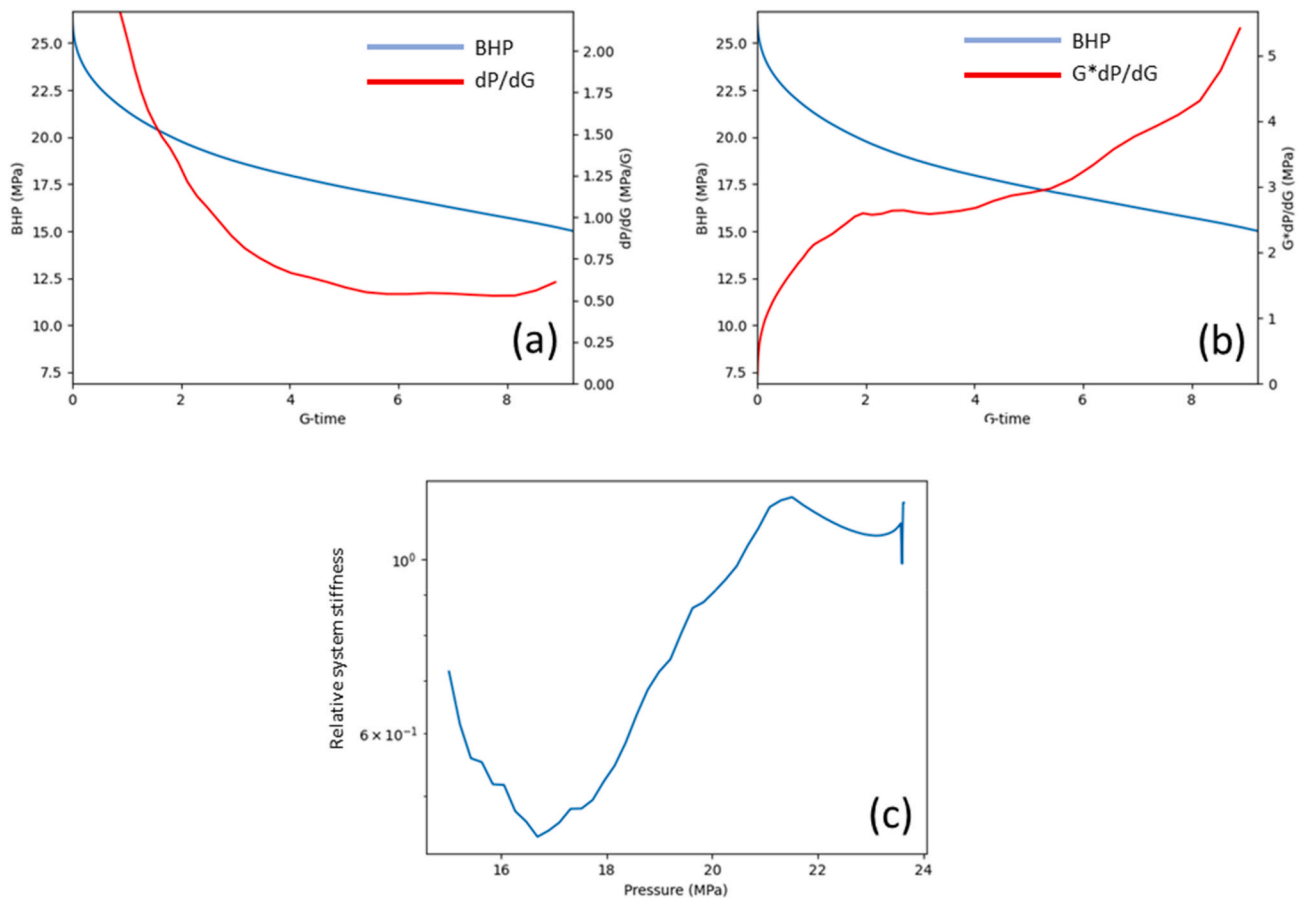
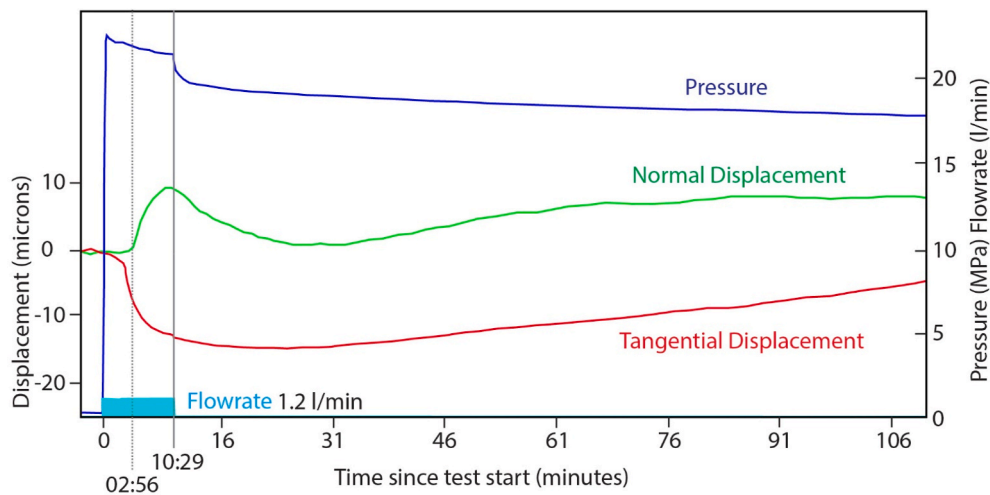


Fig. 10.  $dP/dG$ ,  $G^*dP/dG$ , and relative stiffness plots for E1-I 164 Test 1. The contact pressure is labeled with dashed lines. It is of 21.9 MPa in the  $dP/dG$  plot (for a stress estimate of 21.4 MPa) and 22.1 MPa in the relative stiffness plot. The tangent point cannot be labeled because it is not reached before the end of the transient. A tangent point would have been reached eventually if the shut-in duration had been longer.



**Fig. 11.**  $dP/dG$ ,  $G \cdot dP/dG$ , and relative stiffness plots for E1-I 164 Test 2. There is not a clear ‘compliance’ signature, and so the contact pressure cannot be labeled. The compliance interpretation is ‘rapid closure,’ implying an uncertain range from 20.7 to 24.1 MPa. The tangent point cannot be labeled because it is not reached before the end of the transient. A tangent point would have been reached eventually if the shut-in duration had been longer.



**Fig. 12.** SIMFIP displacement normal and tangential to the activated fracture during TV 4100' Test 4. Displacements are plotted with injection chamber pressure and injection flowrate (note that only a part of the shut-in is plotted on this graph). The tangential displacement is the absolute shear displacement regardless of its direction in the fracture plane.

injection, the first displacement was tangential to the fracture, and displacement normal to the fracture was not detected. Then, at 2:56 min after injection began, the fracture started opening with a normal displacement of about 10  $\mu\text{m}$ . At shut-in there is a smooth normal closure and no clear tangential movement.

Far-field fracture imaging was not performed with the two 4100'

tests. Comparison of imaging logs before and after injection did not show indication of new fractures, but stronger acoustic contrasts were apparent at some of the preexisting fractures after the injections. A newly formed hydraulic fracture would not necessarily be visible from an imaging log performed after the tests. However, the SIMFIP measurements and the OTV/ATV post-test observations were consistent with

reactivation of natural fractures at the wellbore.

Overall, the most likely interpretation is that the two tests performed at the 4100' interval opened a preexisting fracture, and so the closure stress should be interpreted as representing the normal stress on the fracture (which depends on its orientation), rather than the magnitude of the minimum principal stress. This interpretation has some ambiguity because of the possibility that opening mode splay fractures could have propagated off the opening natural fracture.<sup>57</sup> However, in the 4100' tests, there is not any indication from the SIMFIP observations to suggest a far-field reorientation of the strain/deformation field that would be associated with the opening of splay fractures. Our focus in this paper is to compare estimates of the fracture closure pressure from the SIMFIP and the pressure observations, and so regardless of the interpretation of closure pressure with respect to the overall state of stress, we can evaluate the methods based on their ability to estimate closure pressure.

The SIMFIP estimates of closure in Cycle 1 and reopening in Cycle 2 are affected by nonmonotonic behavior evidently caused by complex hydromechanical effects associated with leakage into the formation (Fig. 13). During the Cycle 1 shut-in, the normal displacement drops to near zero at 18.6 MPa, and then goes back up. Estimates of stress from the x-intercept are challenging because the data does not yield a smooth, ideal straight-line, as in the E1-I 164 tests. In Cycle 2, it is not possible to apply the x-intercept because displacement did not reach a minimum or an asymptote. The reopening pressure in Cycle 2 appears to be around 17.7 MPa.

In the  $dp/dG$  plot, the curve reaches a minimum and begins to increase at about 17.6 MPa, yielding a compliance method stress estimate of 17.1 MPa (Fig. 14). The relative stiffness plot shows an upward deflection at around the same pressures, roughly 17.2 MPa. The  $G^*dp/dG$  curve never bends downward and reaches a tangent point, and so the tangent method interpretation is that the fracture never closed during the shut-in, and so the stress is lower than the final measured value of 15.2 MPa.

TV 4100' Test 7 Cycle 1 involved 12.35 min of injection at 2.8 l/min, followed by a 16-h shut-in (Fig. 15). It is believed that injection reactivated one or more natural fractures. Initially, the SIMFIP-measured

displacements were complex because the reactivated fracture was outside the SIMFIP anchors. Nevertheless, the SIMFIP measurements suggest reactivation of a fracture with  $128^\circ/68^\circ$  dip direction/dip angle. After shut-in, normal displacement briefly continued to increase. Subsequently, it settled into a smooth straight line with x-intercept of 17.9 MPa (lower left panel of Fig. 13). At the start of injection for Cycle 2, displacement increased from its minimum at 16.4 MPa (black line on the lower right panel of Fig. 13).

After TV 4100' Test 7 Cycle 2, fluid was immediately flowed back.<sup>58</sup> recommend interpreting flowback tests with a plot of pressure versus cumulative flowback volume. The stress estimate is based on the intersection of straight lines drawn through the linear periods before and after the downward deflection. In Cycle 2, this yields a stress estimate of 18.5 MPa (Fig. 16).

The  $dp/dG$  plot shows what would be termed an 'adequate' indication of closure<sup>35</sup> (Fig. 17). There is an upward deflection in  $dp/dG$ , but it never actually reaches a minimum. The upward deflection occurs at approximately 19.8 MPa (the pick has some degree of subjectivity), suggesting a stress estimate of 19.3 MPa. The relative stiffness plot does not show a clear upward inflection, with the implied relative stiffness increasing steadily as pressure drops.

The  $G^*dp/dG$  curve reaches a tangent point at 18.6 MPa, which is within 0.7 MPa of the compliance method estimate. The SIMFIP estimate is 17.9 MPa, and the flowback test interpretation is 18.5 MPa. Thus, in this case, the methods are within 1.4 MPa of each other, with the compliance interpretation slightly higher than the others.

Table 2 summarizes the results from the different tests. The E1-I 164 tests were performed in the same interval, but the other two tests were performed in different intervals. Table 3 summarizes some of the key details of the tests, such as injection duration and volume.

A statistical comparison from<sup>35</sup> suggests wide variance in the difference between the tangent and compliance methods. This is consistent with the results from this study, where the accuracy of the tangent interpretation was highly variable. If the tangent method was inaccurate by a consistent amount, then it could potentially be adjusted to account for the bias. However, because the inaccuracy is inconsistent, this

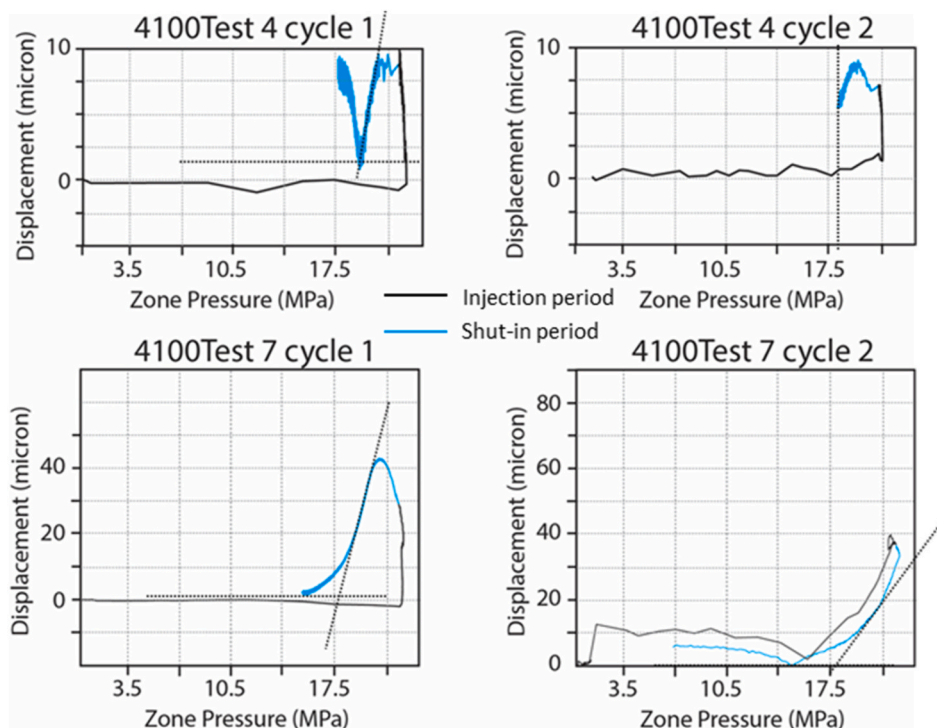
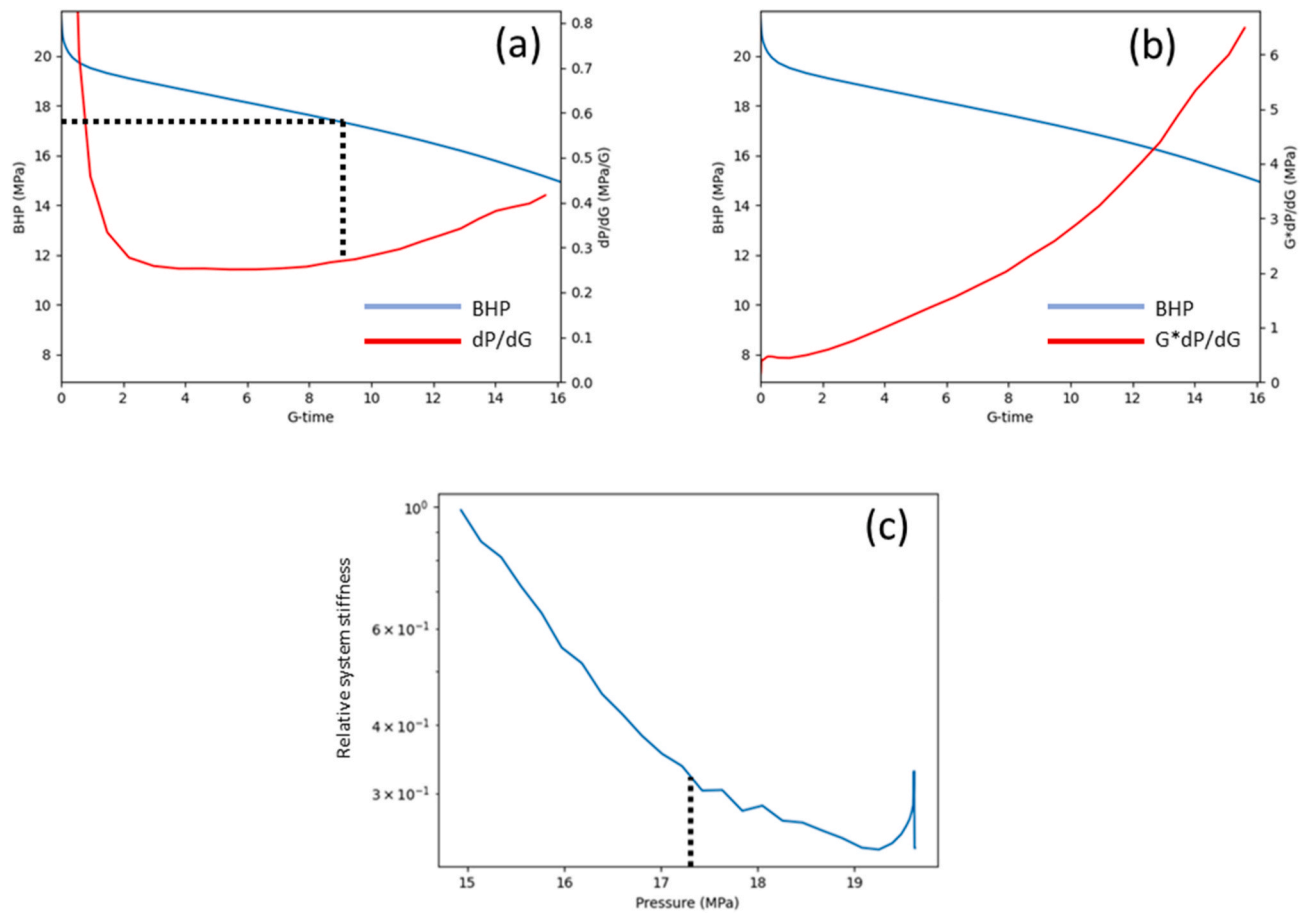
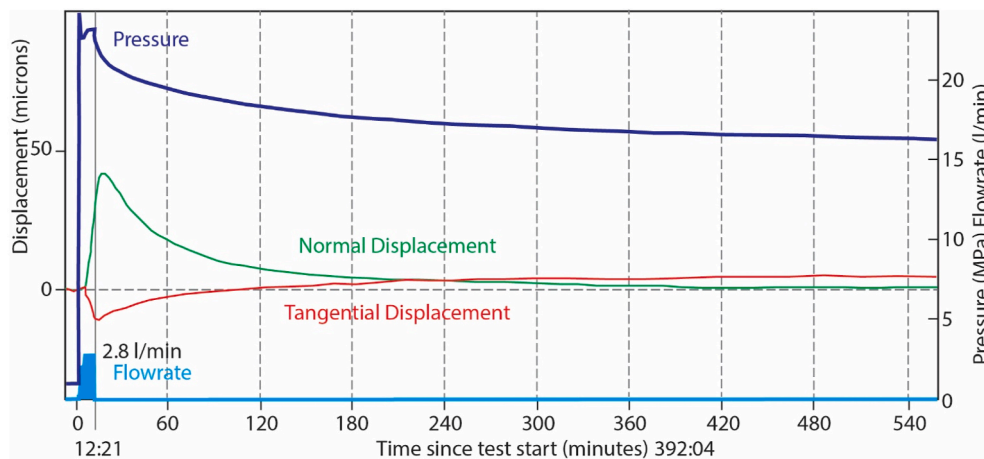


Fig. 13. SIMFIP displacement normal to the activated fracture versus zone pressure for the TV 4100' tests (black is the injection period, blue is the shut-in period). The x-intercept values are unclear in 4100' Test 4. In Test 4 Cycle 1 the displacement reaches a minimum during shut-in at 18.6 MPa. In Test 4 Cycle 2, the reopening and closure curves lift off from a minimum at around 17.7 MPa. In Test 7 Cycles 1 and 2, the x-intercept value is around 17.9 MPa. (For interpretation of the references to colour in this figure legend, the reader is referred to the Web version of this article.)



**Fig. 14.**  $dP/dG$ ,  $G \cdot dP/dG$ , and relative stiffness plots for TV 4100' Test 4. The contact pressure is labeled with dashed lines. It is 17.6 MPa (for a stress estimate of 17.1 MPa) in the  $dP/dG$  plot, and 17.2 MPa in the relative stiffness plot. The tangent point cannot be labeled because it is not reached before the end of the transient. A tangent point would have been reached eventually if the shut-in duration had been longer.



**Fig. 15.** SIMFIP displacement normal and tangential to the activated fracture during TV 4100' Test 7. Displacements are plotted with injection chamber pressure and injection flowrate (note that only a part of the shut-in is plotted on this graph). The tangential displacement is the absolute shear displacement regardless of its direction in the fracture plane.

suggests that the estimate does not have any reliable relationship to the actual stress magnitude. This finding is expected because it has been shown mathematically that the tangent method procedure does not have a theoretical relationship with the process of closure.<sup>16</sup>

### 3.3. Comparison with the <sup>1</sup> and 'deviation from linearity' techniques for estimating stress from shut-in tests

<sup>1</sup> recommend estimating stress with a plot of  $dt/dP$  versus  $P$ . The curve should be fit with three straight lines, and the magnitude of the least principal stress should be estimated from the pressure at the



## Test 7, Cycle 2 Flowback

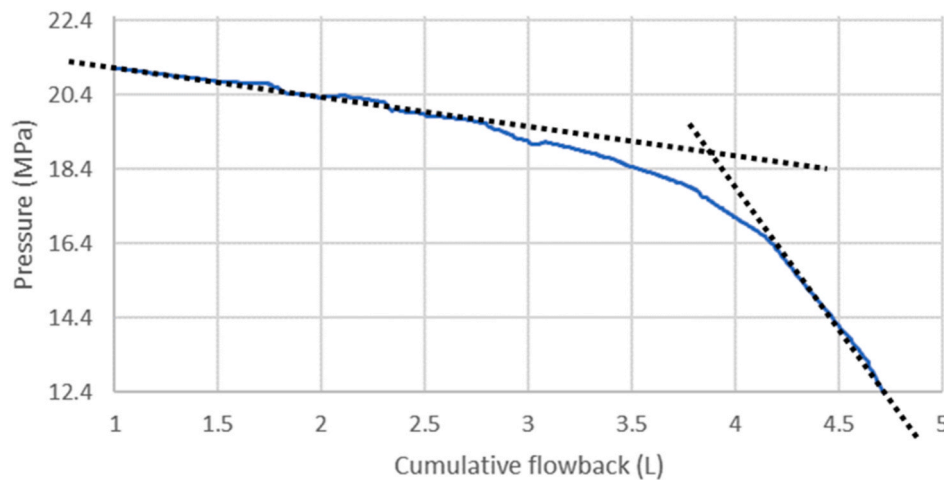


Fig. 16. Pressure versus cumulative flowback volume for the TV 4100' Test 7, Cycle 2 flowback. The lines intersect at 18.5 MPa.

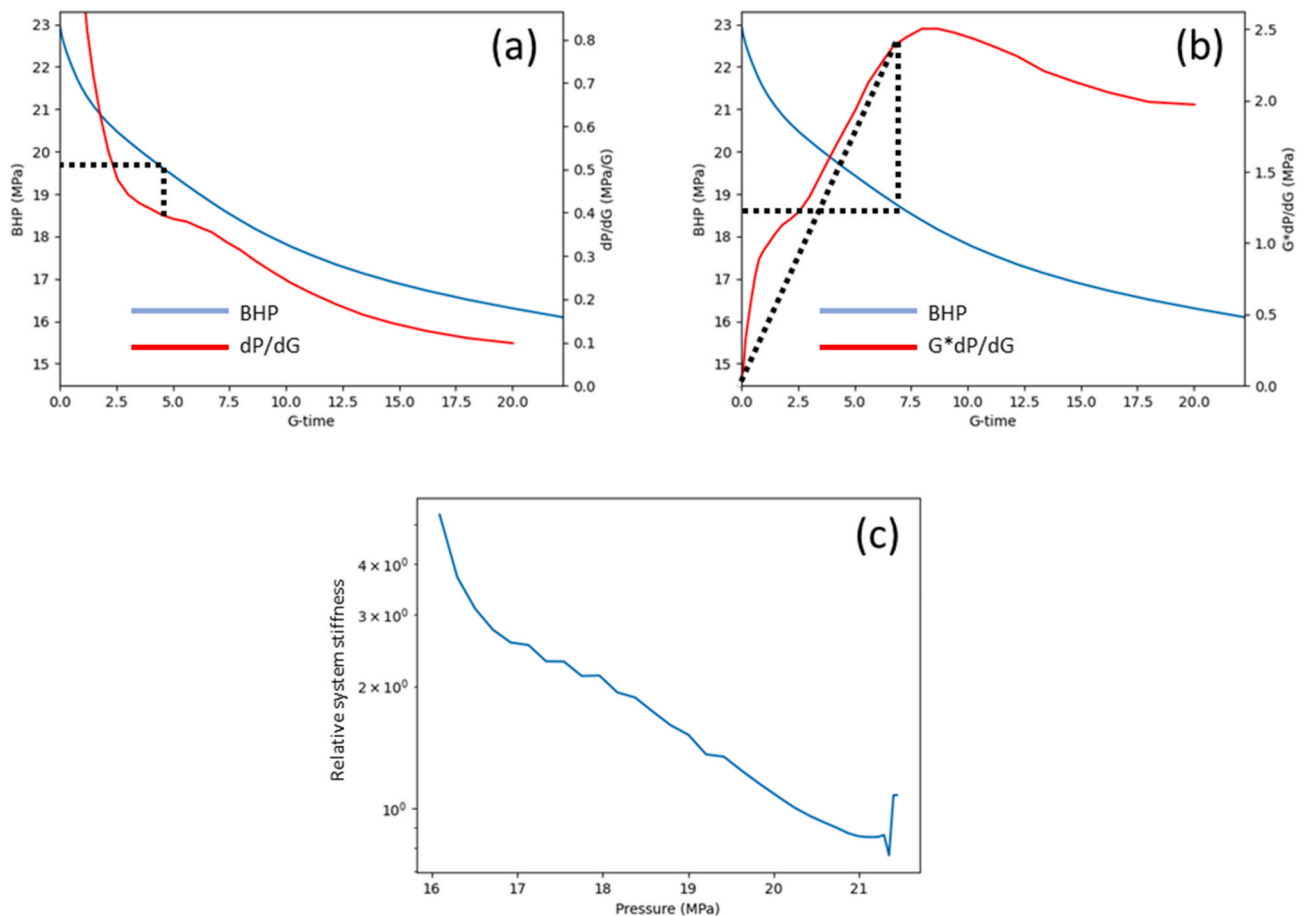


Fig. 17.  $dP/dG$ ,  $G \cdot dP/dG$ , and relative stiffness plots for TV 4100' Test 7. The contact pressure and tangent point are labeled with dashed lines. The contact pressure from the  $dP/dG$  plot is 19.8 MPa (suggesting a stress estimate of 19.3 MPa). The tangent method stress estimate is 18.6 MPa. The relative stiffness plot is ambiguous to interpret, consistent with the only weak inflection observed for  $dP/dG$ .

deviation from linearity on the earliest (highest pressure) straight line<sup>1</sup>; Haimson and Cornet, 1993). Fig. 18 shows the plots for the four tests, and Table 4 summarizes the results. In TV 4100' Test 7, four 'straight line' periods could be identified, and so all four are labeled on the plot. The stress estimate could arguably be picked from the end of either of

the first two straight lines, and so two different possible stress estimates are reported in Table 4. The estimates from the <sup>1</sup> method exceed the SIMFIP estimates by 1.1–3.5 MPa.

Table 4 also summarizes results from estimating stress from the point of deviation from linearity after shut-in on a plot of square root of shut-in

**Table 2**

Comparison of stress estimates from the tangent method, the compliance method, flowback, and the SIMFIP measurements.

Name	Tangent Method	Compliance Method	SIMFIP	Flowback
E1-I 164 Test 1	Less than 20 MPa	21.4 MPa	21.4 MPa	N/A
E1-I 164 Test 2	Less than 15.2 MPa	Rapid closure – 20.7–24.1 MPa	21.4 MPa	N/A
TV 4100' Test 4	Less than 15.2 MPa	17.1 MPa	17.7–18.6 MPa	N/A
TV 4100' Test 7	18.6 MPa	19.3 MPa	17.9 MPa	18.5 MPa

**Table 3**

Injection duration, total injection volume, average injection rate, and shut-in duration for the four tests.

Name	Injection duration (min: sec)	Injection volume (L)	Avg Injection rate (L/min)	Shut-in duration (hours)
E1-I 164 Test 1	10:00	2.1	0.21	2
E1-I 164 Test 2	63:00	23	0.37	15
TV 4100' Test 4	10:29	20.5	1.08	7
TV 4100' Test 7	12:21	45.2	2.15	16

time or G-time (Fig. 1 from 7,29; Figure 7.3 from 9,11).

In both E1-I 164 Test 1 and E1-I 164 Test 2, the first deviation from linearity on the plot of pressure versus G-time occurs at around 24.1 MPa (Figs. 10 and 11), well-above the SIMFIP measured value of 21.4 MPa (Fig. 9). Arguably, the deviation from linearity from E1-I 164 Test 1 could be picked at an even higher stress, 25.5 MPa.

In TV 4100' Test 4, the early deviation from linearity occurs at around 19.0 MPa (Fig. 14). In this case, the interpretation is close to the SIMFIP measured value. In TV 4100' Test 7, the early deviation from linearity occurs at around 21.0 MPa (Fig. 17), well-above the SIMFIP measured value of 18.6 MPa.

In all four tests, it appears that transient effects cause a temporarily elevated rate of pressure decline during the early shut-in period, which

**Table 4**

Comparison of stress estimates from SIMFIP, the method of <sup>1</sup>, and the 'first deviation from linearity.'

Test	SIMFIP stress estimate	Stress estimate from 'first deviation from linearity'	Stress estimate from <sup>1</sup>
E1-I 164 Test 1	21.4 MPa	24.1 or 25.5 MPa	24.7 MPa
E1-I 164 Test 2	21.4 MPa	24.1 MPa	22.5 MPa
TV 4100' Test 4	17.7–18.6 MPa	19.0 MPa	20.4 MPa
TV 4100' Test 7	17.9 MPa	21.0 MPa	21.5 or 19.3 MPa

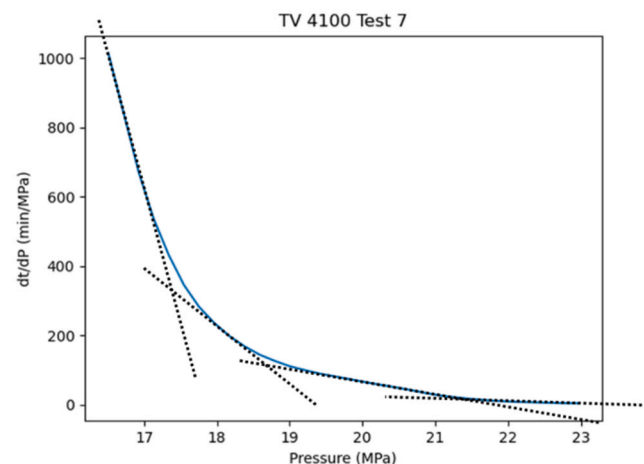
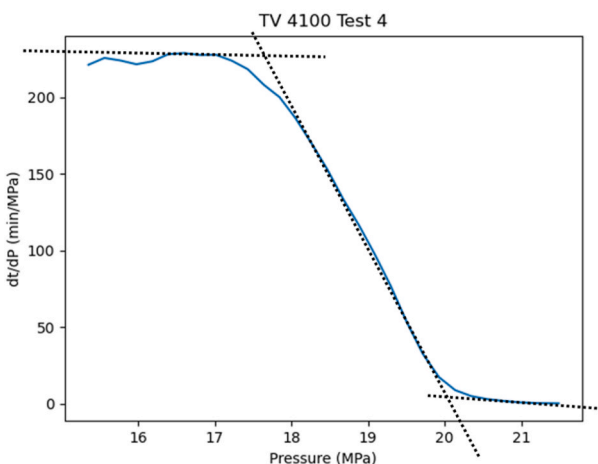
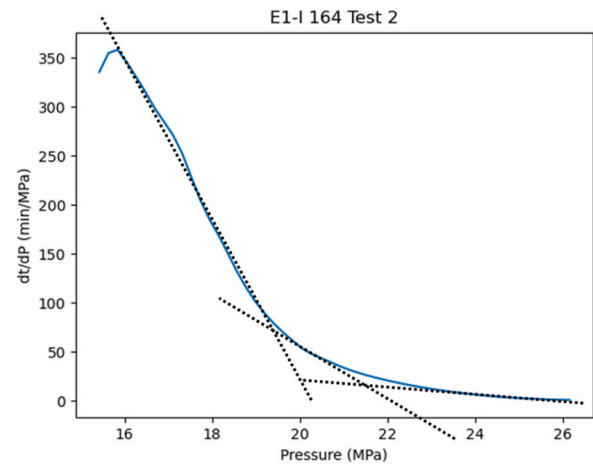
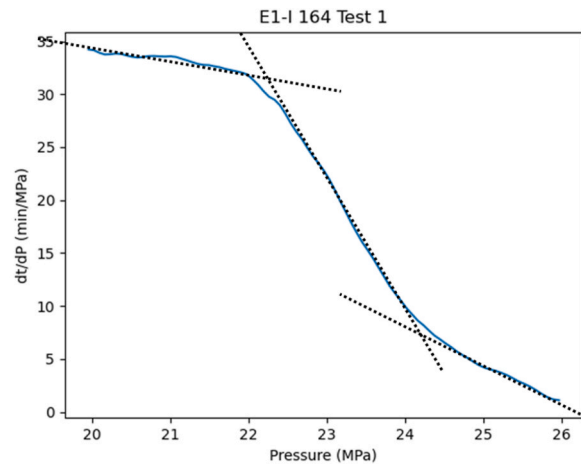


Fig. 18. Plots of  $dt/dP$  versus pressure for the four tests, applying the method from <sup>1</sup>.

affects the accuracy of the <sup>1</sup> and ‘first deviation from linearity’ procedures. Near-wellbore tortuosity (caused either by opening of a natural fracture at the wellbore or complex initiation of hydraulic fractures from the wellbore) is a plausible explanation for this phenomenon. In addition, early-time elevated pressure derivative after shut-in of a fracturing test has been hypothesized to be caused by ‘pressure dependent leakoff’ or ‘tip-extension’.<sup>59</sup>

The method of <sup>1</sup> was recommended in the ISRM procedure from.<sup>8</sup> This procedure lays out carefully controlled test conditions, such as using a wellbore alignment so that a hydraulic fracture can form cleanly at the wellbore (ie, a vertical well in a normal or strike-slip faulting regime). In this ideal configuration, near-wellbore tortuosity should be zero. If the well is not oriented parallel to one of the maximum principal stresses (as in the tests considered in this study), near-wellbore tortuosity may develop and introduce the potential for stress overestimation if using either ‘first deviation from linearity’ or the method from.<sup>1</sup>

As discussed in Section 1.4, early-time pressure drop caused by near-wellbore tortuosity is commonplace in fracturing tests performed for petroleum engineering, at least in non-vertical wells. For example, if applied to the test shown in Fig. 1, the methods of <sup>1</sup> and ‘first deviation from linearity’ would yield large overestimates of the closure pressure, because of the very large magnitude of near-wellbore tortuosity.

<sup>20</sup> also performed a comparison between in-situ strain measurements and pressure transient interpretations of closure. In their results, they observed good accuracy from the method of.<sup>1</sup> Evidently, the accuracy of the method depends on whether or not near-wellbore tortuosity causes elevated pressure derivative at early-time.

### 3.4. Net pressure and fracture size

Microseismic imaging during the E1-I 164 Test 1 injection observed a fracture of “approximately 3 m in diameter”.<sup>55</sup> However, Fig. 7 from <sup>55</sup> shows that seismic events occurred as far as 8 m from the injection well.

During the E1-I 164 Test 2, <sup>55</sup> report that the fracture appears to have propagated towards an offset monitoring well E1-OT. The well was grouted, but it is believed that fluid was nevertheless able to leak off into the well. Fig. 7 from <sup>55</sup> shows that the E1-I 164 Test 2 injection created a fracture with diameter of 10–12 m.

For comparison, we can use a mass balance equation to estimate the fracture size implied by the stress estimates. The volume of fluid injected is equal to the volume of fluid stored in the fracture at shut-in (area times net pressure divided by fracture stiffness) plus the volume of fluid leaked off at shut-in (approximately equal to three times the leakoff coefficient and the square root of injection duration). Assuming a radial crack, we can then write (Equation 40 from <sup>16</sup>):

$$Q_{inj} = \pi R^2 \left[ (ISIP - \sigma_n) \frac{16R}{3\pi E'} + 3(ISIP - P_{res}) \sqrt{\frac{\phi c_t k}{\pi \mu}} \sqrt{t_{inj}} \right], \quad (5)$$

where  $Q_{inj}$  is the volume injected,  $R$  is radius of the crack,  $E'$  is the plane strain modulus (estimated to be 75 GPa),  $P_{res}$  is the reservoir pressure (estimated to be 7 MPa),  $\phi$  is the porosity (estimated to be 4%),  $c_t$  is the total compressibility of the formation (estimated to be  $5e-4$  MPa<sup>-1</sup>),  $k$  is the permeability,  $\mu$  is the viscosity of the fluid (1 cp),  $\sigma_n$  is the normal stress on the fracture, and  $t_{inj}$  is the duration of injection. The permeability is not well-known; however, as a rough estimate, we can use  $1e-19$  m<sup>2</sup>. If the fracture formed instantaneously, the volume of fluid leaked off would be calculated with a factor “4,” not “3.” However, because the fracture propagates over time, and so the leakoff duration is variable along the fracture face, it is common to approximate this effect by using a factor “3” instead of “4.”

Using the stress and radius estimates, we can calculate the implied fracture toughness from stress intensity factor of a circular crack (Equation 2.44 from <sup>37</sup>):

$$K_I = \frac{2}{\pi} (ISIP - \sigma_n) \sqrt{\pi R} \quad (6)$$

Table 5 summarizes the estimated fracture diameter and toughness for the two tests, comparing the results from the compliance and tangent procedures. Microseismic diameter estimates are not available for the two TV 4100' tests.

In the E1-I 164 Test 1, the stress estimate from the compliance method and from the SIMFIP measurements is 21.4 MPa. The estimate from the tangent method in this test is unknown because a tangent point was not reached before the end of the measurements. In E1-I 164 Test 1, the ISIP was approximately 25 MPa, the injection duration was 600 s, and the injection volume was 2.1 L. Given these values, Equation (5) yields a diameter of 3.78 m. With a higher permeability of  $1e-18$  m<sup>2</sup>, it yields a diameter of 3.33 m. With zero leakoff, the equation yields a diameter of 4.03 m. These values are in the range of the 3 m diameter estimated by.<sup>55</sup>

In the E1-I 164 Test 2, the crack is believed to have closed fairly soon after shut-in, probably due to leakoff into the offset observation well. Nevertheless, using the stress estimate from the E1-I 164 Test 1, we can use Equation (5) to estimate the fracture size. In E1-I 164 Test 2, injection volume is 23.08 L, duration is 3795 s, and ISIP is 24.1 MPa. Using the compliance stress estimate of 21.4 MPa and a permeability of  $1e-19$  m<sup>2</sup>, the fracture diameter is calculated to be 9.05 m, close to the estimate of fracture size (which was 10–12 m).

A tangent point was not reached before the end the measurements in Test 2. However, the final pressure measurement was around 15 MPa. If we assume that a tangent point would have been reached shortly after the end of the test, we can use 13 MPa as the tangent method estimate of stress. Using this value, diameter is calculated to be 5.96 m, significantly smaller than observed in the microseismic imaging.

If we use the compliance stress estimate and the ISIP from the E1-I 164 Test 1 and the calculated diameter of 3.78 m, the implied ‘apparent’ toughness is 5.58 MPa-m<sup>1/2</sup>. Using the compliance stress estimate and the ISIP from E1-I 164 Test 2 and the calculated diameter of 9 m, the implied ‘apparent’ toughness is 6.5 MPa-m<sup>1/2</sup>. Using the estimated tangent stress estimate from E1-I 164 Test 2 (13 MPa) and the calculated diameter of 6 m, the implied ‘apparent’ toughness is 21.6 MPa-m<sup>1/2</sup>. Typical laboratory measurements of fracture toughness in rock are in the range of 1.0–2.5 MPa-m<sup>1/2</sup>.

For comparison, if we assume that the crack diameter from E1-I 164 Test 2 was 12 m (the upper limit on the size of the fracture, based on microseismic imaging), we can use Equation (5) to calculate that the net pressure would have had to be 0.9 MPa, for an implied  $\sigma_{hmin}$  value of 23.2 MPa. This would imply a toughness of 2.5 MPa-m<sup>1/2</sup>, which is in the ballpark of laboratory toughness measurements. However, while this is a tempting interpretation, it is difficult to accept because it requires a lower net pressure than observed from the SIMFIP measurements (Fig. 9).

Overall, the calculation accuracy is reasonable, considering that the equation seeks to describe a complex, in-situ fracturing process with only a simple mass-balance and a radial crack assumption. <sup>55</sup> note that the direction of propagation changed during the test, which implies more complexity than implied by a simple ‘radial propagation’ model. The compliance-method implied diameter is about 25% larger than observed in E1-I 164 Test 1 and 10–25% smaller than observed in E1-I 164 Test 2.

Laboratory measurements of toughness typically vary from 1.1 to 3.9 MPa-m<sup>1/2</sup> (Section 5-4.5 from <sup>36</sup>). The implied toughness values from the compliance method interpretations are significantly larger than this range. The tangent-method calculated diameter from the E1-I 164 Test 2 is 40–50% smaller than observed in the microseismic, and the implied toughness value is much larger than the range of typical laboratory values.

These comparisons show the value of having multiple, overlapping, high-quality measurements. The SIMFIP stress estimates and the

**Table 5**

Summary of fracture diameter and toughness estimates for E1-I 164 Tests 1 and 2 from Equations (5) and (6), based on the compliance and tangent estimates.

Test	Microseismic diameter estimate	Diameter from stress estimate (compliance procedure)	Diameter from stress estimate (tangent procedure)	Implied toughness from stress estimate (compliance procedure)	Implied toughness from stress estimate (tangent procedure)
E1-I 164 Test 1	3 m	3.78 m	NA	5.58 MPa-m <sup>1/2</sup>	NA
E1-I 164 Test 2	10–12 m	9.05 m	~6 m	6.5 MPa-m <sup>1/2</sup>	21.6 MPa-m <sup>1/2</sup>

microseismic fracture size estimates can be compared, allowing assumptions to be cross-checked. Additional datasets of this type would be valuable for calculating apparent ‘field-scale’ values of fracture toughness in different formations.

#### 4. Conclusions

In all four tests, the compliance method estimate is reasonably consistent with the fracture closure stress estimate from the SIMFIP measurements. Three of the four tests had clean ‘S’-shaped dP/dG curves, and one - E1-I 164 Test 2 – had a monotonic dP/dG curve that was interpreted as rapid closure. In contrast, the tangent method significantly underestimated the closure stress in three of the four tests. In the fourth test, the tangent method was consistent with the SIMFIP measurements and also close to the compliance interpretation. Overall, the results are consistent with findings from other studies,<sup>15,20,22</sup> which have found that compliance method is reasonably accurate, and that the tangent method tends to underestimate the closure stress.

The ‘first deviation from linearity’ technique tended to overestimate SIMFIP-measured closure stress, evidently because the initial pressure response after shut-in was affected by transient effects such as near-wellbore tortuosity. However, if discarding the initial period of rapid stress drop, the ‘first deviation from linearity’ approach tended to give similar results to the compliance method, and so yielded accurate results.

The method of <sup>1</sup> tended to overestimate SIMFIP-measured closure stress. As with the ‘first deviation from linearity’ approach, it was affected by early-time transient effects. In the ISRM procedure,<sup>8</sup> recommend the method for use in carefully controlled test procedures to ensure axial hydraulic fracture initiation. None of the four tests considered in this paper included axial fracture initiation. In many practical situations, particularly in the petroleum/geothermal applications with deep, costly boreholes (which are not drilled solely for the purpose of measuring stress), it is not practical to meet all of the requirements of the procedures from.<sup>8</sup> In these non-ideal cases, methods such as <sup>1</sup> may be vulnerable to overestimating the closure stress, because they can be affected by near-wellbore tortuosity.

Within coarse bounds, the microseismically observed fracture geometries are consistent with the fracture sizes calculated from the net pressure observations and the assumption of a single circular fracture. The implied apparent fracture toughness values are 2-3x higher than typical values measured in the lab. This finding is consistent with literature observations of elevated apparent fracture toughness from field-scale fracturing tests.

#### Declaration of competing interest

The authors declare that they have no known competing financial interests or personal relationships that could have appeared to influence the work reported in this paper.

#### Data availability

The data can be downloaded from the OpenEI Geothermal Data Repository <[https://gdr.openet.org/egs\\_collab](https://gdr.openet.org/egs_collab)>.

#### Acknowledgements

This material was based upon work supported by the U.S. Department of Energy, Office of Energy Efficiency and Renewable Energy (EERE), Office of Technology Development, Geothermal Technologies Office, under Award Number DE-AC02-05CH11231 with LBNL, by Lawrence Livermore National Laboratory under Contract DE-AC52-07NA27344, and other awards to other national laboratories. The United States Government retains, and the publisher, by accepting the article for publication, acknowledges that the United States Government retains a non-exclusive, paid-up, irrevocable, world-wide license to publish or reproduce the published form of this manuscript, or allow others to do so, for United States Government purposes. The research supporting this work took place in whole or in part at the Sanford Underground Research Facility in Lead, South Dakota. The assistance of the Sanford Underground Research Facility and its personnel in providing physical access and general logistical and technical support is gratefully acknowledged. Thank you to two anonymous reviewers and the technical editor for their helpful feedback on the manuscript.

#### References

- Hayashi Kazuo, Haimson Bezael C. Characteristics of shut-in curves in hydraulic fracturing stress measurements and determination of in situ minimum compressive stress. *J Geophys Res.* 1991;96(B11).
- Hubbert MK, Willis DG. Mechanics of hydraulic fracturing. *J Petrol Technol.* 1957;9 (6):153–168.
- Godbey JK, Hodges HD. Pressure measurements during formation fracturing operations. *Petrol Trans AIME.* 1958;213:65–69.
- Kehle Ralph O. The determination of tectonic stresses through analysis of hydraulic well fracturing. *J Geophys Res.* 1964;69(2):259–273.
- Haimson Bezael, Fairhurst Charles. Initiation and extension of hydraulic fractures in rocks. *Soc Petrol Eng J.* 1967;7(3):310–318.
- Hickman Stephen H, Zoback Mark D. The interpretation of hydraulic fracturing pressure-time data for in-situ stress determination. In: Zoback MD, Haimson BC, eds. *Hydraulic Fracturing Measurements*. Washington D.C.: National Academy Press; 1983: 44–54.
- Nolte Kenneth. Application of fracture design based on pressure analysis. *SPE Prod Eng.* 1988;3(1):31–42.
- Haimson BC, Cornet F. ISRM Suggested Methods for rock stress estimation Part 3: hydraulic fracturing (HF) and/or hydraulic testing of pre-existing fractures (HTFP). *Int J Rock Mech Min Sci.* 2003;40:1011–1020.
- Zoback Mark. *Reservoir Geomechanics*. Cambridge University Press; 2007.
- Cramer DD, Nguyen DH. Diagnostic fracture injection testing tactics in unconventional reservoirs. In: *SPE 163863. Paper Presented at the SPE Hydraulic Fracturing Technology Conference*. 2013 (Woodlands, TX).
- Schmitt Douglas R, Haimson Bezael. Hydraulic fracturing stress measurements in deep holes. In: Feng Xia-Ting, ed. *From Rock Mechanics and Engineering*. vol. 1. 2017.
- Barree RD, Barree VL, Craig DP. Holistic fracture diagnostics: consistent interpretation of prefracture injection tests using multiple analysis methods. *SPE 107877. SPE Prod Oper.* 2009;24(3):396–406.
- Barree RD, Miskimins JL, Gilbert JV. Diagnostic fracture injection tests: common mistakes, misfires, and misdiagnoses. *SPE Prod Oper.* 2015;30(2):84–98.
- McClure Mark W, Blyton Christopher AJ, Jung Hojung, Sharma Mukul M. The effect of changing fracture compliance on pressure transient behavior during diagnostic fracture injection tests. In: *SPE 170956. Paper Presented at the Annual Technical Conference and Exhibition*. 2014 (Amsterdam, The Netherlands).
- McClure Mark W, Jung Hojung, Cramer Dave D, Sharma Mukul M. The fracture compliance method for picking closure pressure from diagnostic fracture injection tests. *SPE J.* 2016;21(4):1321–1339.
- McClure Mark, Bammidi Vidya, Craig Cipolla, et al. A collaborative study on DFTT interpretation: integrating modeling, field data, and analytical techniques. In: *Paper Presented at the Unconventional Resources Technology Conference*. 2019 (Denver, Colorado).
- Craig DP, Barree RD, Warpinski NR, Blasingame TA. Fracture closure stress: reexamining field and laboratory experiments of fracture closure using modern



- interpretation methodologies. *SPE 187038. Paper presented at the SPE Annual Technical Conference and Exhibition*. 2017 (San Antonio, TX).
- 18 Wang HanYi, Sharma Mukul M. New variable compliance method for estimating in-situ stress and leak-off from DFIT data. In: *SPE 187348. Paper Presented at the Annual Technical Conference and Exhibition*. 2017 (San Antonio, TX).
  - 19 McClure Mark. Discussion of the paper "SPE-187038-MS: fracture closure stress: reexamining field and laboratory experiments of fracture closure using modern interpretation methodologies.". *arXiv:1904*. 2019, 07126.
  - 20 Dutler Nathan, Valley Benoit, Gischig Valentin, et al. Hydromechanical insight of fracture opening and closure during in-situ hydraulic fracturing in crystalline rock. *Int J Rock Mech Min Sci*. 2020;135.
  - 21 Buijs H ernan. DFIT: an interdisciplinary validation of fracture closure pressure interpretation across multiple basins. In: *SPE 206239. Paper Presented at the Annual Technical Conference and Exhibition*. 2021 (Dubai, UAE).
  - 22 Br oker Kai, Ma Xiaodong. Estimating the least principal stress in a granitic rock mass: systematic mini-frac tests and elaborated pressure transient analysis. *Rock Mech Rock Eng*. 2022;391.
  - 23 Ye Zhi, Ahmad Ghassemi. Reexamining in-situ stress interpretation using laboratory hydraulic fracturing experiments. In: *Paper Presented at the 48<sup>th</sup> Workshop on Geothermal Reservoir Engineering*. Stanford University; 2023.
  - 24 Kneafsey TJ, Blankenship D, Knox HA, et al, the EGS Collab team. EGS Collab project: status and progress. In: *Paper Presented at the 44<sup>th</sup> Workshop on Geothermal Reservoir Engineering*. Stanford University; 2019.
  - 25 Kneafsey TJ, Blankenship D, Dobson PF, et al, the EGS Collab team. The EGS Collab project: learnings from experiment 1. In: *Paper Presented at the 45<sup>th</sup> Workshop on Geothermal Reservoir Engineering*. Stanford University; 2020.
  - 26 Guglielmi Yves, Cappa Frederic, Lan on Herv , et al. ISRM suggested method for step-rate injection method for fracture in-situ Properties (SIMFIP): using a 3-components borehole deformation sensor. *Rock Mech Rock Eng*. 2013;47:303–311.
  - 27 Guglielmi Y, Cook P, Soom F, Schoenball M, Dobson P, Kneafsey T. In situ continuous monitoring of borehole displacements induced by stimulated hydrofracture growth. *Geophys Res Lett*. 2021;48.
  - 28 Guglielmi Yves, McClure Mark, Burghardt Jeffrey, et al, The EGS Collab Team. Estimating stress from fracture injection tests: comparing pressure transient interpretations with in-situ strain measurements. In: *Proceedings, 47<sup>th</sup> Workshop on Geothermal Reservoir Engineering*. Stanford University; 2022.
  - 29 Castillo JL. Modified fracture pressure decline analysis including pressure-dependent leakoff. In: *SPE 16417. Paper Presented at the SPE/DOE Low Permeability Reservoir Symposium*. 1987 (Denver, CO).
  - 30 Mack Mark G, Warpinski Norman R. Mechanics of hydraulic fracturing. In: Economides Michael, Nolte Kenneth, eds. *Reservoir Stimulation*. 2000.
  - 31 Delaney Paul T, Pollard David D, Ziony Joseph I, McKee Edwin H. Field relations between dikes and joints: emplacement processes and paleostress analysis. *J Geophys Res*. 1986;91(B5):4920–4938.
  - 32 Scholz Christopher H. A note on the scaling relations for opening mode fractures in rock. *J Struct Geol*. 2010;32.
  - 33 Fu Wei, Morris Joseph, Fu Pengcheng, et al. Developing upscaling approach for swarming hydraulic fractures observed at hydraulic fracturing test site through multiscale simulations. In: *SPE 199689. Paper Presented at the SPE Hydraulic Fracturing Technology Conference and Exhibition*. 2020 (The Woodlands, TX).
  - 34 Shylapobersky J. Energy analysis of hydraulic fracturing. In: *Paper Presented at the 26<sup>th</sup> US Symposium on Rock Mechanics*. South Dakota: Rapid City; 1985.
  - 35 McClure Mark, Fowler Garrett, Picone Matteo. Best practices in DFIT interpretation: comparative analysis of 62 DFITs from nine different shale plays. In: *SPE 205297. Paper Presented at the International Hydraulic Fracturing Technology Conference and Exhibition*. Oman: Muscat; 2022.
  - 36 Smith MB, Shylapobersky JW. Basics of hydraulic fracturing. In: Economides Michael, Nolte Kenneth, eds. *Reservoir Stimulation*. 2000.
  - 37 Anderson TL. *Fracture Mechanics: Fundamentals and Applications*. CRC Press; 2005.
  - 38 Shahri Mojtaba, Tucker Andrew, Rice Craig, et al. High fidelity fibre-optic observations and resultant fracture modeling in support of planarity. In: *SPE 204172. Paper Presented at the Hydraulic Fracturing Technology Conference and Exhibition*. 2021 (The Woodlands, TX).
  - 39 Ratcliff Dave, McClure Mark, Fowler Garrett, Elliot Brendan, Austin Qualls. Modelling of parent child well interactions. In: *SPE 209152. Paper Presented at the Hydraulic Fracturing Technology Conference and Exhibition*. 2022 (The Woodlands, TX).
  - 40 Pudugramam Sriram, Irvin Rohan J, McClure Mark, et al. Optimizing well spacing and completion design using simulation models calibrated to the Hydraulic Fracture Test Site 2 (HFTS-2) Dataset. In: *Paper Presented at the Unconventional Resources Technology Conference*. 2022 (Houston, Texas).
  - 41 Howard George C, Fast CR. Optimum fluid characteristics for fracture extension. In: *Paper Presented at the Spring Meeting of the Mid-Continental District, Division of Production*. 1957 (Tulsa, OK).
  - 42 Nolte Kenneth. Determination of fracture parameters from fracturing pressure decline. In: *SPE 8341. Paper Presented at the Annual Fall Technical Conference and Exhibition of the Society of Petroleum Engineers*. 1979 (Las Vegas, NV).
  - 43 Gulrajani Sunil N, Nolte KG. Chapter 9: fracture evaluation using pressure diagnostics. In: Economides Michael J, Nolte Kenneth G, eds. *Reservoir Stimulation*. Wiley; 2000.
  - 44 Valko PP, Economides MJ. Fluid-leakoff delineation in high-permeability fracturing. *SPE Prod Facil*. 1999;14(2):117–130.
  - 45 Marongiu-Porcu Matteo, Retnanto Albertus, Economides Michael J, Ehlig-Economides Christine. Comprehensive fracture calibration test design. In: *SPE 168634. Paper Presented at the SPE Hydraulic Fracturing Technology Conference*. 2014 (The Woodlands, TX).
  - 46 McClure Mark. The spurious deflection on log-log superposition-time derivative plots of diagnostic fracture-injection tests. *SPE Reservoir Eval Eng*. 2017;20(4):1045–1055.
  - 47 Sneddon IN. The distribution of stress in the neighborhood of a crack in an elastic solid. *Proc Royal Soc Lond Ser A*. 1946;187(1009):229–260.
  - 48 Jaeger John, Cook NG, Zimmerman Robert. *Fundamentals of Rock Mechanics*. fourth ed. Wiley-Blackwell; 2007.
  - 49 Malik Mayank, Schwartz Ken, Moelhoff Ken, Vinay K, Mishra. Microfracturing in tight rocks: a Delaware Basin case study. In: *SPE 169009. Paper Presented at the SPE Unconventional Resources Conference*. 2014 (The Woodlands, TX).
  - 50 Singh A, Zoback M, Dobson PF, et al, the EGS Collab team. Slip tendency analysis of fracture networks to determine suitability of candidate testbeds for the EGS Collab hydroshear experiment. *Trans Geoth Resour Counc*. 2019;43:405–424.
  - 51 Wang HF, Lee MY, Doe T, Haimson BC, Oldenburg CM, Dobson PF. In-situ stress measurement at 1550-meters depth at the KISMET test site in Lead. In: *S.D. Paper Presented at the 51st US Rock Mechanics/Geomechanics Symposium*. 2017 (San Francisco, California).
  - 52 Guglielmi Y, Nussbaum C, Rutqvist J, Cappa F, Jeanne P, Birkholzer J. Estimating perturbed stress from 3-D borehole displacements induced by fluid injection in fractured or faulted shales. *Geophys J Int*. 2020;221:1684–1695.
  - 53 Kakurina M, Guglielmi Y, Nussbaum C, Valley B. In situ direct displacement information on fault reactivation during fluid injection. *Rock Mech Rock Eng*. 2020;53:4313–4328.
  - 54 Barton N, Bandis S, Bakhtar K. Strength, deformation and conductivity coupling of rock joints. *Int J Rock Mech Min Sci Geomech Abstracts*. 1985;22(3):121–140.
  - 55 Schoenball Martin, Ajo-Franklin Jonathan B, Blankenship Doug, et al. Creation of a mixed-mode fracture network at mesoscale through hydraulic fracturing and shear stimulation. *J Geophys Res*. 2020;125(12), e2020JB019807.
  - 56 Fu Pengcheng, et al. Close observation of hydraulic fracturing at EGS Collab Experiment 1: fracture trajectory, microseismic interpretations, and the role of natural fractures. *J Geophys Res*. 2021;126(7), e2020JB020840.
  - 57 Jung Hojung, Sharma Mukul M, Cramer Dave D, Oakes Sean, McClure Mark W. Re-examining interpretations of non-ideal behavior during diagnostics fracture injection tests. *J Petrol Sci Eng*. 2016;145:114–136.
  - 58 Plahn SV, Nolte KG, Thompson LG, Miska S. A quantitative investigation of the fracture pump-in/flowback test. *SPE Prod Facil*. 1997;12(1):20–27.
  - 59 Nolte Kenneth G. Fracturing-pressure analysis for nonideal behavior. *J Petrol Technol*. 1991;43(2):210–218.
  - 60 Kneafsey TJ, Blankenship D, Dobson PF, et al, the EGS Collab team. The EGS Collab – discoveries and lessons from an Underground experiment series. In: *PROCEEDINGS, 48<sup>th</sup> Workshop on Geothermal Reservoir Engineering*. Stanford, California: Stanford University; 2023. February 6-8, 2023 SGP-TR-224.